Title
Limited Carbon Cycle Response to Increased Sulfide Weathering Due to Oxygen Feedback

Journal
Geophysical Research Letters, 48(19)

ISSN
0094-8276

Authors
Maffre, Pierre
Swanson-Hysell, Nicholas L
Goddéris, Yves

Publication Date
2021-10-16

DOI
10.1029/2021gl094589

Peer reviewed

Limited Carbon Cycle Response to Increased Sulfide Weathering due to Oxygen Feedback

Pierre Maffre[1], Nicholas Swanson-Hysell[1], Yves Goddéris[2]

[1]University of California, Berkeley, department of Earth and Planetary Sciences
[2]Géosciences Environnement Toulouse, CNRS—Université Paul Sabatier - IRD, 31400 Toulouse, France.

Key Points:

- The effect of oxidative sulfide weathering on CO_2 is dependent on the coupled oxygen-carbon-sulfur cycles
- Due to feedbacks, an increase in sulfide weathering will switch from a transient C source to a C sink on geologically short timescales
- This behavior is robust for a large range of oxygen feedback strengths

Citation:
Maffre, P., Swanson-Hysell, N. L., Goddéris, Y. (2021). Limited carbon cycle response to increased sulfide weathering due to oxygen feedback. Geophysical Research Letters, 48, e2021GL094589. https://doi.org/10.1029/2021GL094589

Corresponding author: Pierre Maffre, `maffre@berkeley.edu`

Abstract

The chemical weathering of sulfide-bearing rocks can result in the dissolution of carbonate rocks leading to degassing of CO_2 to the atmosphere. While this process has been argued to be a significant geologic source of CO_2, it also perturbs the geological cycles of oxygen and sulfur, triggering a cascade of geochemical feedbacks. Using a numerical model of geochemical cycles and climate, we found that due to feedbacks on atmospheric oxygen associated with the organic carbon cycle, an increase of sulfide weathering leads to a limited source of CO_2 followed by a longer sink of CO_2. This result is due to the stoichiometry of sulfide weathering where more O_2 is consumed than CO_2 is released. If sulfide weathering increases progressively on a geological timescale, the duration of the carbon source is extended, but its magnitude is negligible before it becomes a carbon sink.

Plain Language Summary

Earth's climate has changed through time from being warmer than today for millions of years to being colder than today for millions of years. Climate on Earth over these long time periods is set by the balance of carbon dioxide coming into the ocean and atmosphere and carbon dioxide going out. Knowing how big different sources of carbon dioxide to Earth's surface is important for understanding what has caused Earth's climate to change through time. While carbon dioxide coming out of volcanoes is usually thought to be the most important source, there are other sources. One such source is when the common mineral pyrite (sometimes known as "fools gold") gets exposed in mountains and rusts through exposure to oxygen. This process results in acid which dissolves other rocks that can release carbon. However, when pyrite rusts it consumes oxygen. At lower oxygen levels, organic carbon that is made through photosynthesis is more likely to be preserved and buried in sediments. As a result, the overall effect of pyrite weathering on carbon dioxide levels is limited and can actually cause them to go down by a small amount.

1 Introduction

On million-year timescales, the sources and sinks of CO_2 on Earth's surface need to be balanced (Berner & Caldeira, 1997). Volcanism and metamorphic outgassing are typically considered the main sources of CO_2 to the long-term carbon cycle. However, recent attention has been drawn to the CO_2 source associated with sulfuric acid produced by sulfide mineral weathering (e.g., pyrite) dissolving carbonate rocks (Spence & Telmer, 2005; Torres et al., 2014, 2017; Emberson et al., 2018; Shukla et al., 2018; Kölling et al., 2019; Blattmann et al., 2019). The sulfide oxidation flux has been re-estimated at higher values than previously thought (Calmels et al., 2007; Burke et al., 2018), and is correlated to erosion rate (Calmels et al., 2007; Torres et al., 2016, 2017; Hilton & West, 2020; Bufe et al., 2021). This process could be important in the evolution of Earth's climate and is relevant in association with orogenies that uplift sulfide-bearing sedimentary lithologies. Torres et al. (2014) proposed that sulfide oxidation coupled to terrestrial carbonate dissolution could be a sustained carbon source, owing to the relatively long residence time of sulfate in the ocean (10–15 Myr). The authors argued that this process could be a missing source of CO_2 in the Cenozoic Era, accompanied by a decrease of atmospheric oxygen (as sulfide oxidation is a sink of O_2).

A modification of the sulfide oxidation flux would also modify the interrelated geochemical cycles of carbon, oxygen, and sulfur. The overall response of atmosphere-ocean geochemistry to a perturbation of sulfide oxidation therefore depends on the strength and timing of the different feedbacks in these geochemical cycles.

The existence of a negative feedback stabilizing atmospheric CO_2 has been acknowledged for several decades, the so-called "weathering thermostat" of the climatic feedback

on silicate weathering being presented as the best candidate (Walker et al., 1981; Berner et al., 1983). Because of the short residence time of carbon in the ocean atmosphere system (100 kyr), this feedback must operate within a few hundred thousand years (Berner & Caldeira, 1997). Despite large-scale orogenic activity over the Cenozoic, oxygen levels are estimated to be relatively stable, between 20 % and 24 % of atmosphere volume (Mills et al., 2016). The estimated range of variation since the Carboniferous is $15 - 35$ % (Berner et al., 2003). This stability suggests the presence of a substantial negative feedback operating on atmospheric oxygen levels. Organic carbon burial in marine sediments is thought to prevent oxygen levels from getting too low, either through a reduction of O_2-dependent carbon oxidation during early diagenesis (Betts & Holland, 1991) or through enhanced productivity due to reduced phosphorus burial under anoxic conditions (Van Cappellen & Ingall, 1996). Land vegetation processes, including terrestrial wildfires, provide additional negative feedbacks (Lenton & Watson, 2000). The feedbacks on oceanic sulfate concentrations are not straight-forward. The formation of massive sulfate evaporites (e.g., gypsum, anhydrite) are more sensitive to the particular paleogeographic configurations that lead to restricted basins in arid environments than on sulfate concentrations. Nevertheless, precipitation of sulfide minerals through sulfate reduction likely depends on sulfate concentration (Canfield & Farquhar, 2009) and this may hold true for the precipitation disseminated sulfate minerals as well. These processes would provide negative feedback that prevents unbounded drift. Hence, geochemical cycle models, such as COPSE (Lenton et al., 2018), generally assume those fluxes to be proportional to sulfate concentration.

Given the existence of these feedbacks, one cannot straightforwardly determine how CO_2 and climate would evolve in the million years following a perturbation of sulfide weathering. The present study addresses this question with a modeling approach. Using the coupled geochemical cycles/climate model GEOCLIM (Goddéris & Joachimski, 2004; Donnadieu et al., 2006; Goddéris & Donnadieu, 2019), we explore the sensitivity of transient climate evolution to an increase of sulfide weathering on million year timescales.

Sulfide oxidative weathering can be described by the generalized equation:

$$\frac{1}{2}FeS_2 + \frac{15}{8}O_2 + \frac{7}{4}H_2O \longrightarrow \frac{1}{2}Fe(OH)_3 + H_2SO_4 \tag{1}$$

The released sulfuric acid typically dissolves surrounding carbonate minerals:

$$H_2SO_4 + CaCO_3 \longrightarrow Ca^{2+} + {SO_4}^{2-} + CO_2 + H_2O \tag{2}$$

If not, it may alter the riverine or oceanic water alkalinity balance and carbonate precipitation, leading to the same budget. Alternatively, sulfuric acid might dissolve silicate minerals, the budget would then be different:

$$H_2SO_4 + CaSiO_3 \longrightarrow Ca^{2+} + {SO_4}^{2-} + SiO_2 + H_2O \tag{3}$$

Eventually, the cycle is closed by sulfate reduction and sulfide precipitation in marine sediment that can be described by the generalized equation:

$${SO_4}^{2-} + \frac{1}{2}Fe(OH)_3 + 2\,CH_2O + \frac{1}{8}O_2 \longrightarrow \frac{1}{2}FeS_2 + 2\,{HCO_3}^{-} + \frac{7}{4}H_2O \tag{4}$$

Followed by carbonate precipitation:

$${Ca_2}^{+} + 2{HCO_3}^{-} \longrightarrow CaCO_3 + CO_2 + H_2O \tag{5}$$

These last two processes balance the alkalinity and sulfur budgets, but not the carbon and oxygen ones. The burial of organic carbon produced by the biosphere finally close the budgets (expressed here with a stoichiometry comparable to previous equations):

$$2CO_2 + 2H_2O \longrightarrow 2CH_2O + 2O_2 \tag{6}$$

2 Materials and Methods

2.1 Model

We used the global spatially-resolved geochemical cycle model COMBINE that is a component of the GEOCLIM Earth system model (Goddéris & Joachimski, 2004; Donnadieu et al., 2006; Goddéris & Donnadieu, 2019). The model code is available on Zenodo (`https://doi.org/10.5281/zenodo.5246622`). GEOCLIM simulates the cycles of geochemical species (including carbon, oxygen, alkalinity and phosphorus) in ocean-atmosphere reservoirs that are discretized in 10 "boxes" (9 oceanic, 1 atmospheric), and is coupled to climate model results that are used to compute continental fluxes at the resolution of the climate model. GEOCLIM is designed for multi-million year simulations while being fully dynamic (i.e., no steady-state assumption is made regarding the chemical species) and parameterizes fast processes, like ocean mixing and water column sedimentation. The coupled modeling of continental processes, climate, and ocean biogeochemistry enables the model to address the impact of increased sulfide weathering on the carbon cycle.

This study combines recent improvements of the GEOCLIM model and implements a simplified sulfur cycle. A more complete description of the model and the calibration procedure can be found in the Supporting Information (Text S1, S2 and S3).

GEOCLIM's continental weathering module computes physical erosion, silicate, carbonate, petrogenic organic carbon and phosphorus weathering, and terrestrial organic carbon export. Surface bedrock is divided into six lithological classes, following Park et al. (2020), utilizing the data compilation of Hartmann and Moosdorf (2012). The erosion and silicate weathering components are similar to Park et al. (2020), but solve the equations dynamically instead of assuming a steady-state regolith. Terrestrial biospheric organic carbon export is an addition with respect to published versions of GEOCLIM and uses the formulation of Galy et al. (2015). Regarding petrogenic organic carbon and sulfide weathering, following recent studies that indicate a near linear relationship between those two fluxes and erosion rates (Calmels et al., 2007; Hilton et al., 2014), we considered them to be proportional to the modeled erosion rate, with prescribed organic matter content and C:S ratio. As a simplification, we assumed that sulfuric acid released by sulfide oxidation dissolves carbonate and silicate rocks, in addition to chemical weathering driven by carbonic acid, with the same carbonate/silicate flux ratio as for "carbonic" weathering.

The climate simulations used by the weathering module are the same as in Park et al. (2020). The GFDL CM2.0 General Circulation Model (Geophysical Fluid Dynamics Laboratory Coupled Model version 2.0, Delworth et al., 2006) was run, at 1, 2 and 4 times pre-industrial CO_2 with other boundary conditions set to be constant at pre-industrial values.

For the purpose of this study, a simplified sulfur cycle has been implemented in GEOCLIM. We assume that the only processes modifying the sulfur budget are the continental sulfide oxidation, and the reduction of sulfate in marine sediments. All other fluxes (sulfur degassing, evaporite dissolution and precipitation) are set at steady-state values. This simplification of the pathways is implemented given the difficulties in accurately representing evaporite precipitation with no explicit evaporitic basins.

The preservation of deposited organic carbon in marine sediments is mostly controlled by the local sedimentation rate. Organic carbon burial efficiency is modulated by O_2 and ${SO_4}^{2-}$ concentrations, providing a negative feedback for those element cycles (Betts & Holland, 1991; Hartnett et al., 1998; Canfield & Farquhar, 2009). These processes are simulated using an early diagenesis module (Simon et al., 2007). It consists of a steady-state reactive-transport model calculating at each time step of GEOCLIM the amount of organic matter escaping oxidation such that it is buried in the sediment. Organic matter moves downward, at the sedimentation rate, through a biotur-

bated layer (starting at the surface of sediment), where it is oxidized by O_2, and through a "sulfate reduction layer", where it is oxidized by ${SO_4}^{2-}$. H_2S generated by this process reacts with iron to form sulfide minerals (Equation 4). Oxidation rate is considered to be proportional to the concentration of organic matter in the sediment times the concentration of the oxidant (O_2 or ${SO_4}^{2-}$) in the local GEOCLIM ocean box. Hence, the oxidation flux F_{oxid} in a given layer is:

$$F_{oxid} = \frac{F_{in}}{1 + w/kh[\mathrm{X}]} \tag{7}$$

With F_{in} the incoming flux of C at the top of the layer, w the sedimentation rate, h the layer thickness, [X] the concentration of the oxidant (O_2 or ${SO_4}^{2-}$), and k the rate constant.

The GEOCLIM model was calibrated to reproduce pre-industrial conditions using modern fields of slope and lithology and climate fields from climate model runs at $1\times CO_2$, under the assumption of steady-state. While this assumption is questionable for long residence time species (S and O) it should be considered as a neutral hypothesis, given the difficulties to estimate the current imbalance of the geochemical cycles (e.g., Burke et al., 2018). Starting the numerical experiments at steady-state is preferable as otherwise the assumed non-steady-state trajectory will be superimposed on responses to an imposed increase in sulfide weathering.

2.2 Design of Perturbations

The perturbations we applied to the pre-industrial steady-state consist of increasing by 50% the sulfide weathering flux, either instantaneously at $t = 0$ (abrupt perturbation) or progressively over 40 Myr (progressive perturbation). This perturbation is scaled to the "background" sulfide weathering, which means it evolves with climate evolution (with erosion being parameterized to be dependent on runoff rates in addition to slope). In other words, this perturbation is equivalent to increasing by 50% the amount of sulfides in surface rock exposures, without changing its organic carbon content. Two end-members concerning the fate of the additional sulfuric acid are presented here: additional dissolution of carbonate and additional dissolution of silicate, referred as "carbonate" and "silicate" sulfuric weathering perturbations. More scenarios are discussed in the Supporting Information (Text S5 and Figures S4–S8).

2.3 Oxygen feedback sensitivity experiments

We conducted additional experiments where we varied the strength of the oxygen feedback. In GEOCLIM, two simulated processes are responsible of this feedback: the O_2-dependent oxidation of organic matter in marine sediment and the burial of phosphorus with organic matter. The C:P burial ratio depends on the degree of anoxicity (Van Cappellen & Ingall, 1994):

$$(\mathrm{C:P})_{burial} = \frac{(\mathrm{C:P})_{oxic} \cdot (\mathrm{C:P})_{anoxic}}{(1 - DOA) \cdot (\mathrm{C:P})_{anoxic} + DOA \cdot (\mathrm{C:P})_{oxic}} \tag{8}$$

In other words, the amount of P buried for a given amount of buried C varies linearly with the degree of anoxicity (DOA) between the two end-members.

The DOA represents the fraction of the basin that is anoxic. It varies from 1 (fully anoxic basin) to 0 (fully oxic basin). It only depends on local oxygen concentration, using the relation of Van Cappellen and Ingall (1994, polynomial fit of Figure 4A of their contribution). Roughly speaking, it linearly decreases from 1 for $[O_2] = 0$ mol/m^3 to 0 for $[O_2] = 0.4$ mol/m^3 (see Figure S1).

Less oxygen in seawater leads to less burial of phosphorus, leading to higher primary productivity via P upwelling, and more organic C burial.

This case is the reference oxygen feedback scenario ("ref"). To vary the strength of the oxygen feedback, we added or removed O_2 dependencies to several processes. We made the hydrothermal phosphorus sink (Wheat et al., 1996)—independent of oxygen in "reference" case—dependent to $[O_2]$ (case "feedback+1"), or dependent to $[O_2]^2$ (case "feedback+2"). We further made terrestrial biospheric organic carbon export dependent to $(p_{O_2})^{-0.5}$ (case "feedback+3") or to $(p_{O_2})^{-1}$ (case "feedback+4"). To reduce the oxygen feedback strength, we imposed a constant DOA (case "feedback-1"), independent of oxygen concentration. We further reduced the O_2 dependence in Equation 7 to $[O_2]^{0.5}$ (case "feedback-2"). Finally, we removed the O_2 dependence in Equation 7, leaving no oxygen feedback in the model (case "no feedback"). These modifications serve as a way to modulate the overall oxygen feedback strength given that it has considerable uncertainty.

To quantify the strength of the oxygen feedback for each of those different scenarios, we computed the steady-state p_{O_2} after a 50% increase in petrogenic carbon weathering, everything else—including phosphorus weathering—unchanged. This "perturbed" steady-state p_{O_2} ranges from 0.44 to 0.68 PAL, the reference case being 0.56 PAL (see Text S4, Table S3 and Figure S2 in Supporting Information).

3 Results

3.1 Abrupt perturbation

Starting from geochemical steady-state, we applied at $t = 0$ a step-function increase of sulfide weathering and carbonate dissolution by released sulfuric acid.

The immediate response is an increase of atmospheric CO_2 (Figure 1a) because of the direct CO_2 release. This excess CO_2 causes a rapid drop of oceanic pH (Figure 1g) of 0.1, leading to a reduction of carbonate precipitation (Figure 1b) tempering the atmospheric CO_2 rise by storing dissolved inorganic carbon in the ocean.

The main negative feedback, in terms of amplitude, arises from the organic carbon cycle (Figure 1c). On the timescale of 1 Myr, the rise of temperature leads to lower oxygen solubility in seawater, and more importantly, higher phosphorus delivery through weathering (see Figures S3 and S10), both increasing organic carbon burial flux by 0.42 Tmol/yr. The silicate weathering flux also contributes to the CO_2 drawdown, but by a smaller amount — 0.22 Tmol/yr in the same time interval (Figure 1b). These two fluxes stabilize pCO_2 at $\sim$ 380 eq ppm.

On longer timescales (1 to 10 Myr), the progressive decline of pO_2 consumed by sulfide oxidation results in an increase of DOA in the ocean. Consequently, the preservation of organic C in sediment and the C:P ratio of the buried organic matter both increase. Higher primary productivity (given enhanced phosphorus availibility, see Figure S3) and burial efficiency maintain the high organic carbon burial, consuming atmospheric CO_2. As a result, pCO_2 drops below its initial value around 14 Myr, long before the atmospheric oxygen level stabilizes (around 35 Myr, Figure 1f).

The sulfur cycle stays imbalanced by 0.1 Tmol/yr after 50 Myr of run (see Figures 1h and S5). There are several reasons for this result. First, the modeled sulfur cycle residence time is significantly longer than the oxygen one (30 Myr vs. 5 Myr). Second, the sulfur negative feedback is not linear. The main control on sulfate reduction is the amount of organic carbon buried (Raiswell & Berner, 1986). Therefore, as organic carbon burial increases in the first couple of million years of simulation, so does sulfate reduction (see Figure S5). The ratio of organic C versus S burial fluxes into the marine sediments stays

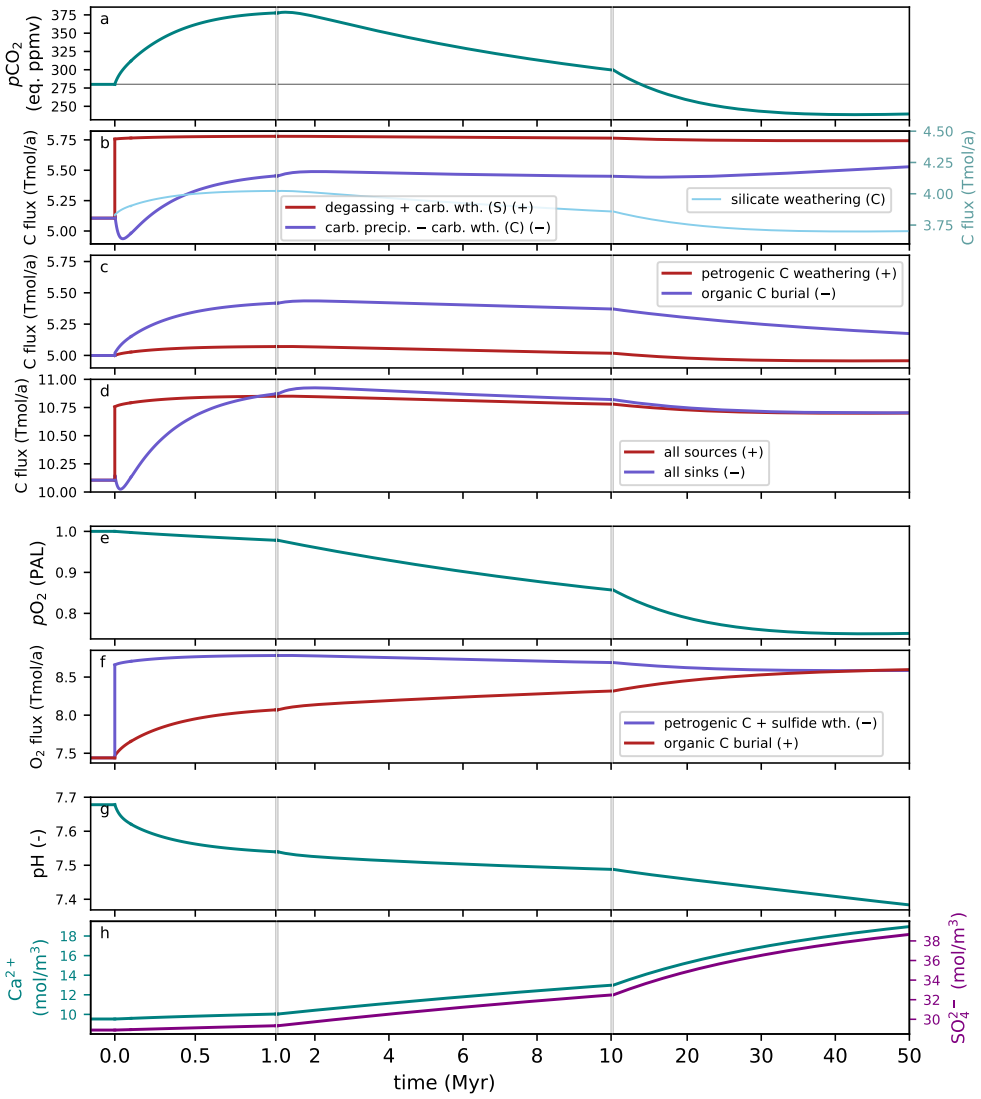

Figure 1. Time evolution of major ocean-atmosphere chemical species and fluxes following an "abrupt carbonate sulfuric weathering" perturbation applied at $t = 0$ and sustained. Fluxes are shown as their absolute value with a positive source indicated with a (+) in the legend and a negative sink indicated with a (−). a. atmospheric partial pressure of CO_2, expressed in equivalent ppmv (theoretical mixing ratio if all other gases amounts were kept unchanged). b. inorganic carbon fluxes (left axis) and silicate weathering flux (right axis). c. organic carbon fluxes. d. sum of carbon sources and sinks. e. atmospheric partial pressure of O_2, expressed relatively to present one (PAL). f. oxygen fluxes. g. mean ocean pH. h. mean ocean calcium (left axis) and sulfate (right axis) concentration. "wth" is the abbreviation of "weathering". When ambiguous, weathering by carbonic or sulfuric acid is specified by C or S (respectively). In panels b. and h., the left and right y axis have the same scale.

roughly constant during the phase of increasing organic carbon burial. Yet, the achievement of steady-state of all cycles requires a different C:S burial ratio. Steady-state is reached when organic carbon burial has increased by 16%, which buffers the oxygen perturba-

tion, and sulfate reduction has increased by 50%, which buffers the sulfate perturbation. Accordingly, the C:S burial ratio progressively decreases in order to reach steady-state. To achieve this multi-cycle steady-state (including sulfur), the calculated oceanic sulfate must rise significantly given its weak control on the C:S burial ratio. An accelerated equilibrium simulation shows that sulfate concentration must increase up to 43.3 mol/m^3 to balance the perturbation. Given that the sulfur cycle is imbalanced at 50 Myr of run, it would take approximately another 50 Myr to achieve steady-state.

In the last 20 Myr of simulation, oxygen and sulfur cycles are nearly at steady-state, while accommodating the long-term drift of the sulfur cycle (Figure 1). Atmospheric pO_2 decreases to 0.75 PAL for organic carbon burial to balance the oxygen sink (Figure 1 e and f). Because sulfide weathering still exceeds sulfate reduction, the resulting net O_2 sink is compensated by an organic C burial flux higher than the sum of petrogenic C oxidation, carbonate sulfuric weathering and sulfate reduction C fluxes. These coupled processes result in a net C sink, that is compensated by a reduced silicate weathering flux, itself controlled by lower than pre-industrial atmospheric CO_2 (239 eq ppm, corresponding to a global cooling of 0.45 °C, see Figure 1 a and d). Eventually, when the sulfur cycle reaches steady-state, atmospheric CO_2 will return to its initial value, since only a perturbation of the inorganic carbon cycle is able to modify the steady-state CO_2.

3.2 Progressive perturbation

This abrupt perturbation experiment is helpful to understand the processes, but a more realistic sulfide weathering perturbation would occur gradually. We conducted a second experiment where we linearly increase the sulfide weathering (rigorously, the amount of sulfide in exhumed rocks) over 40 million years, up to the same value of +50%. Given that the onset of this perturbation occurs on a similar time-scale to that of the oxygen feedback, the global warming associated with it is virtually nonexistent (+15.5 eq ppm of CO_2 corresponding to 0.15 °C of warming), and the CO_2 drops below the initial level at 35 Myr instead of 13.7 Myr (Figure 2a, orange curves).

3.3 Silicate dissolution

We consider here the second scenario where the additional sulfuric acid released by the sulfide weathering perturbation dissolves "new" silicate minerals (Equation 3). In that scenario, sulfuric acid is neutralized without additional source of carbon, so the atmospheric CO_2 continually decreases, because of the organic C dependent oxygen feedback, to a much lower value than in the "carbonate" scenario (110 eq ppm of CO_2, 2.6 °C of cooling, Figure 2a, blue curves). Atmospheric O_2 also stabilizes at lower value (0.55 PAL, Figure 2b), because of both reduced phosphorus weathering and higher seawater oxygen solubility in colder climate. Considering a progressive perturbation rather than an abrupt one only delays the stabilization of the oxygen and carbon cycles (Figure 2 a and b, blue curves).

3.4 Effect of oxygen feedback

Because the oxygen feedback is responsible for sulfide weathering perturbation to switch from a net source to a net sink of C, we investigated the sensitivity of our simulations to that feedback's strength. We repeated this experiment of "carbonate sulfide weathering" perturbation with different oxygen feedback strengths (see Methods, and Supporting Information, Text S4).

In the carbonate sulfuric weathering abrupt perturbation experiment, despite a relatively large scatter of pO_2 level at "steady-state" (0.6–0.83 PAL, Figure 2e), the CO_2 peak and its timing is a robust feature, with maximum pCO_2 of 365–400 eq ppm, reached at 1–1.6 Myr (Figure 2c). Only if all oxygen feedbacks are removed can the sulfide per-

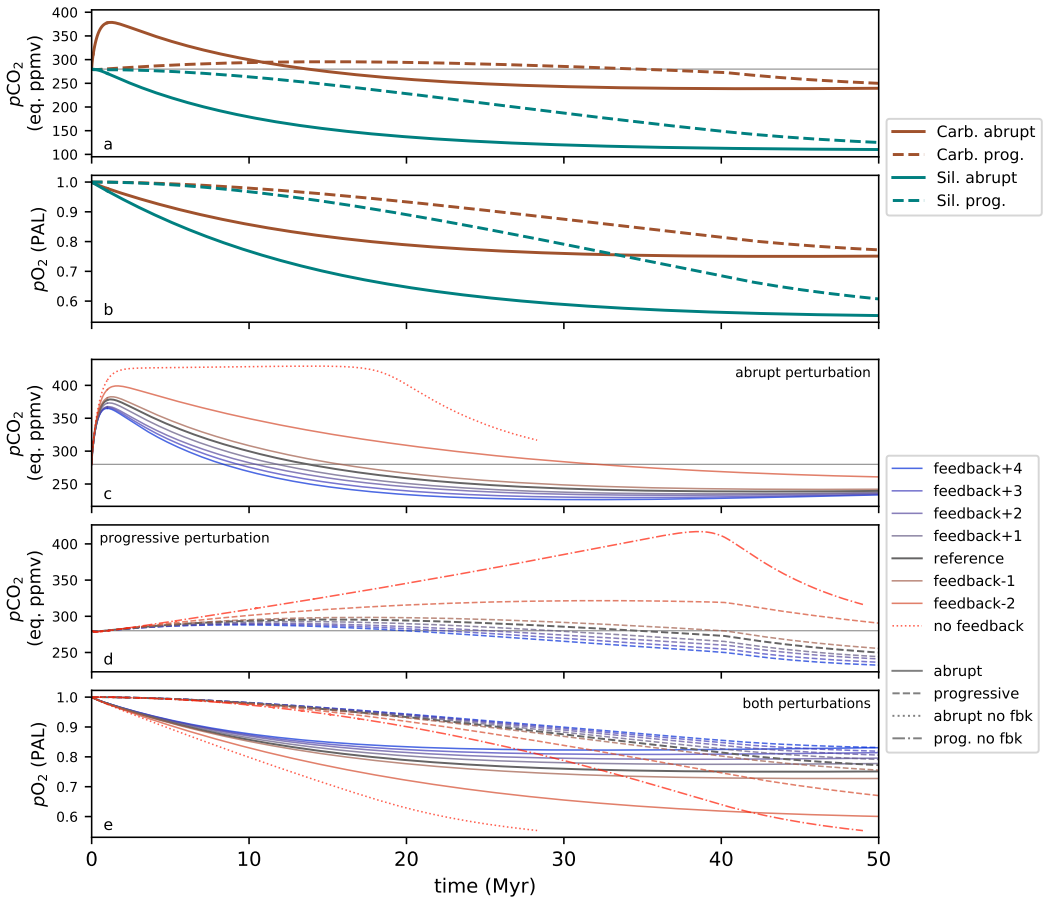

Figure 2. Time evolution of atmospheric CO_2 (a., c. and d.) and O_2 (b. and e.) for different simulation setups. a. and b. "carbonate" or "silicate sulfuric weathering" perturbation, abrupt or progressive over 40 Myr, c., d. and e. "carbonate sulfuric weathering" perturbation, abrupt (c. and e.) or progressive (d. and e.) with different strengths of O_2 feedback. The same color codes are applied in a. and b., and in c., d. and e. The units of pCO_2 and pO_2 are the same as in Figure 1.

turbation generate a sustained source of carbon, maintaining high CO_2 level for tens of million years. However, in that theoretical experiment, CO_2 eventually declines near 17 Myr because the epicontinental waters below the photic zone becomes fully anoxic (O_2 concentration lower than 8 mmol/m^3) and organic particles are no longer efficiently remineralized in the water column, which increases the organic carbon burial flux. At 28 Myr, oxygen mass-balance can no longer be satisfied because the organic carbon oxidation during early diagenesis (made independent of O_2 concentration in this scenario) exceeds the amount of oxygen available in the basin.

All other sensitivity experiments show a drop of CO_2 below pre-industrial level, occurring between 8 Myr and 16 Myr, except for the "feedback-2" case where the CO_2 decrease is much slower than the others.

In the case of a progressive perturbation, the CO_2 peak remains negligible (Figure 2d) while a similar persistent lower CO_2 is achieved after the sulfide weathering ceases to increase, with the exception of the "feedback-2" and "no feedback" cases.

4 Discussion and Conclusion

4.1 Robustness of oxygen feedback modeling

The strength and timing of the oxygen feedback is the key element controlling the CO_2 evolution in our experiments. Several mechanisms have been suggested to explain the negative feedback needed for the oxygen cycle, and their representation in GEOCLIM relies on empirical parameterizations.

Based on observed correlations between organic C content in marine sediment, sedimentation rate, and dissolved O_2 concentration, Betts and Holland (1991) found that the feedback provided by O_2-dependent organic C preservation in sediment would alone yield an atmospheric pO_2 of 0.1 atm (i.e., 0.48 PAL) for a 50% increase in oxidative weathering, in their "maximum slope" (i.e., maximum feedback strength) case. This value is close to our "feedback-1" scenario (0.51 PAL, see Table S3), where O_2-dependent organic C preservation is the only feedback.

Other ocean-based feedbacks involved the removal of oceanic phosphorus with organic matter, adsorbed on iron hydroxides and calcium-bound, all providing a negative feedback; denitrification, on the other hand, provides a positive feedback (Lenton & Watson, 2000). In GEOCLIM ("reference" scenario), these feedbacks are parameterized with the degree of anoxicity, without explicit representation of iron speciation, nor organic matter and Ca binding. The nitrogen cycle and potential nitrogen-limitation on primary productivity is also ignored. Considering only the oceanic P-based feedbacks, Van Cappellen and Ingall (1996) found that pO_2 would drop down to 0.59 PAL after a 50% increase of oxidative weathering through uplift (the additional P delivered by enhanced continental weathering caused by uplift being delayed in their model). This pO_2 decrease is smaller than in our "reference" scenario.

Lenton and Watson (2000) argued that considering all these feedbacks together is needed to be consistent with the evidence of geologic oxygen stability. They also discussed land-based oxygen feedbacks, though more to explain the upper bound of oxygen variations. Land-based feedbacks are absent in the GEOCLIM "reference" scenario, we added a pO_2 dependence of terrestrial biospheric organic C export in scenarios "feedback+3" and "feedback+4".

Given that the oxygen feedback in GEOCLIM "reference" is weaker than the literature estimates, the "high CO_2" scenarios (feedback-2 and feedback-1) are unlikely, and the ones with lower CO_2 than "reference" are more probable.

4.2 Simplification of sulfur cycle

Sulfide burial is interpreted to be dependent on sulfate concentration (Canfield & Farquhar, 2009). However, how oceanic sulfate concentration controls sulfide burial is poorly known making it difficult to confidently parameterize. The much longer time required for sulfate reduction to balance sulfide weathering, compared to oxygen stabilization time, is another key element of the CO_2 evolution in our experiments, because of the stoichiometry of $-15/8$ O_2 for $+1$ CO_2 (Equation 1 and 2). Two arguments support this long sulfur balancing time: the long residence time of the "reduced" sulfur sub-cycle (30 Myr) compared to oxygen (5.1 Myr), and the consistent C:S ratio observed in sediments (Berner & Raiswell, 1983; Kurtz et al., 2003) suggesting a weak control of sulfate concentration on this ratio; a ratio that needs to be modified in order for sulfur cycle to be balanced in our experiments.

It may be argued that the actual sulfur residence time is shorter because of the "evaporitic" sub-cycle, whose fluxes should respond to sulfate perturbations, and could potentially affect long-term climate (Shields & Mills, 2021). Considering an evaporitic sulfate weathering flux of 1.5 Tmol/yr (Burke et al., 2018) would reduce the residence time

of sulfur to 14 Myr. However, increasing evaporitic sulfate precipitation in response to sulfate and calcium concentration rise would not change the O_2:CO_2 stoichiometry, and the main effect is to further delay the rise of oceanic sulfate concentration needed for balancing the "reduced" sulfur sub-cycle. This would act in favor of an even more pronounced and longer CO_2 sink resulting from an increase in sulfide weathering.

4.3 Sulfide weathering and petrogenic organic carbon weathering

Investigating the effect of an increase of sulfide weathering alone is a rather theoretical study. In Earth history, sulfide weathering is likely to have varied concomitantly with petrogenic organic carbon weathering, as sulfides are dominantly found in organic-rich sedimentary rocks. Both of their weathering rates have been shown to increase quasi-linearly with erosion rate (Calmels et al., 2007; Hilton et al., 2014). Decoupling of petrogenic organic carbon and sulfide weathering fluxes is still possible, by exhuming rocks with a lower C:S ratio than Earth surface average. Additionally, uplift and erosion influence on carbon fluxes is not restricted to sulfide and organic carbon weathering given concurrent changes in silicate weathering (Hilton & West, 2020), and uplift also affects ocean-atmosphere circulation, indirectly modifying weathering rates (Maffre, Ladant, Donnadieu, et al., 2018; Maffre, Ladant, Moquet, et al., 2018).

Nevertheless, a proportional increase of sulfide and petrogenic organic carbon weathering (presented in Supporting Information, Text S5 and Figure S9) have a different impact. With an unchanged C:S ratio of global weathering fluxes, the rise of organic carbon burial and associate sulfate reduction fluxes caused by oxygen decline balances both oxygen and sulfur cycle in roughly the same time. This switches the ratio of $-15/8$ O_2 for $+1$ CO_2 toward a -2:$+2$ ratio. Hence, CO_2 only undergoes a relaxation towards its pre-perturbation value instead of dropping below that value.

4.4 Consequences for paleoclimatic evolution

Sulfide oxidation linked to carbonate weathering is a source of CO_2, but it is also a sink of O_2, resulting in additional organic carbon burial and removal of CO_2. Because of its larger effect on oxygen, an increase of sulfide weathering alone is, on the long term, a sink of CO_2. Its source effect is either limited in time for a rapid perturbation, or limited in amplitude for a progressive perturbation. This sink would be further enhanced if evaporite sulfate precipitation delays the rise of oceanic ${SO_4}^{2-}$, or if part of the additional sulfuric acid dissolves "new" silicates (i.e., silicates that would not have been dissolved by carbonic acid otherwise). The magnitude of such potential additional silicate weathering, however, is largely unknown. It is relevant for actively erosive environments, where "carbonic" silicate weathering is limited by kinetics rather than by the amount of exposed minerals, and therefore, less likely to be reduced by mineral consumption by enhanced "sulfuric" weathering.

Our findings suggest that sulfide weathering can not be solely interpreted as a missing source of carbon. Rather through the effects of oxygen and carbon cycle feedbacks it can instead be a sink. While there are significant uncertainties on the strength of the oxygen feedback, if there is a feedback on atmospheric oxygen levels through the carbon cycle, the decrease in atmospheric oxygen levels resulting from sulfide weathering will result in enhanced organic carbon burial that is a sink of carbon dioxide. This result highlights the need to consider the cascading biogeochemical effects of a process such as sulfide weathering. While reconstructing the forcing of long-term climate change remains a major challenge, the subdued effect of sulfide weathering on the carbon cycle emphasizes the relative importance of CO_2 outgassing and silicate weathering.

Acknowledgments

Project research was supported by NSF Frontier Research in Earth Sciences (FRES) Grant 1925990. The authors thank Daniel Stolper and members of the FRES project team for fruitful discussions. We thank the two anonymous reviewers whose constructive input improved the manuscript. The authors declare no conflict of interest. All code associated with this study is archived on Zenodo (`https://doi.org/10.5281/zenodo.5246622`; DOI: 10.5281/zenodo.5246622).

References

Arndt, S., Regnier, P., Goddéris, Y., & Donnadieu, Y. (2011). GEOCLIM reloaded (v 1.0): a new coupled earth system model for past climate change. *Geoscientific Model Development*, *4*(2), 451–481. doi: 10.5194/gmd-4-451-2011

Berner, R. A., Beerling, D. J., Dudley, R., Robinson, J. M., & Wildman, R. A. (2003). Phanerozoic Atmospheric Oxygen. *Annual Review of Earth and Planetary Sciences*, *31*(1), 105–134. doi: 10.1146/annurev.earth.31.100901.141329

Berner, R. A., & Caldeira, K. (1997). The need for mass balance and feedback in the geochemical carbon cycle. *Geology*, *25*(10), 955–956.

Berner, R. A., Lasaga, A. C., & Garrels, R. M. (1983). The carbonate-silicate geochemical cycle and its effect on atmospheric carbon dioxide over the past 100 million years. *American Journal of Science*, *283*(7), 641–683. doi: 10.2475/ajs.283.7.641

Berner, R. A., & Raiswell, R. (1983). Burial of organic carbon and pyrite sulfur in sediments over Phanerozoic time: a new theory. *Geochimica et Cosmochimica Acta*, *47*(5), 855–862. doi: 10.1016/0016-7037(83)90151-5

Betts, J. N., & Holland, H. D. (1991). The oxygen content of ocean bottom waters, the burial efficiency of organic carbon, and the regulation of atmospheric oxygen. *Global and Planetary Change*, *5*(1-2), 5–18. doi: 10.1016/0921-8181(91)90123-E

Blattmann, T. M., Wang, S.-L., Lupker, M., Märki, L., Haghipour, N., Wacker, L., ... Eglinton, T. I. (2019). Sulphuric acid-mediated weathering on Taiwan buffers geological atmospheric carbon sinks. *Scientific Reports*, *9*(1), 2945. doi: 10.1038/s41598-019-39272-5

Bufe, A., Hovius, N., Emberson, R., Rugenstein, J. K. C., Galy, A., Hassenruck-Gudipati, H. J., & Chang, J.-M. (2021). Co-variation of silicate, carbonate and sulfide weathering drives CO_2 release with erosion. *Nature Geoscience*, *14*(4), 211–216. doi: 10.1038/s41561-021-00714-3

Burke, A., Present, T. M., Paris, G., Rae, E. C., Sandilands, B. H., Gaillardet, J., ... Adkins, J. F. (2018). Sulfur isotopes in rivers: Insights into global weathering budgets, pyrite oxidation, and the modern sulfur cycle. *Earth and Planetary Science Letters*, *496*, 168–177. doi: 10.1016/j.epsl.2018.05.022

Calmels, D., Gaillardet, J., Brenot, A., & France-Lanord, C. (2007). Sustained sulfide oxidation by physical erosion processes in the Mackenzie River basin: Climatic perspectives. *Geology*, *35*(11), 1003. doi: 10.1130/G24132A.1

Canfield, D. E., & Farquhar, J. (2009). Animal evolution, bioturbation, and the sulfate concentration of the oceans. *Proceedings of the National Academy of Sciences*, *106*(20), 8123–8127. doi: 10.1073/pnas.0902037106

Davy, P., & Crave, A. (2000). Upscaling local-scale transport processes in large-scale relief dynamics. *Physics and Chemistry of the Earth, Part A: Solid Earth and Geodesy*, *25*(6-7), 533–541. doi: 10.1016/S1464-1895(00)00082-X

Delworth, T. L., Broccoli, A. J., Rosati, A., Stouffer, R. J., Balaji, V., Beesley, J. A., ... Zhang, R. (2006). GFDL's CM2 Global Coupled Climate Models. Part I: Formulation and Simulation Characteristics. *Journal of Climate*, *19*(5), 643–674. doi: 10.1175/JCLI3629.1

Donnadieu, Y., Goddéris, Y., Pierrehumbert, R., Dromart, G., Fluteau, F., & Jacob,

R. (2006). A GEOCLIM simulation of climatic and biogeochemical consequences of Pangea breakup. *Geochemistry, Geophysics, Geosystems*, *7*(11). doi: 10.1029/2006GC001278

Emberson, R., Galy, A., & Hovius, N. (2018). Weathering of Reactive Mineral Phases in Landslides Acts as a Source of Carbon Dioxide in Mountain Belts. *Journal of Geophysical Research: Earth Surface*, *123*(10), 2695–2713. doi: 10.1029/2018JF004672

Filippelli, G. M. (2002). The Global Phosphorus Cycle. *Reviews in Mineralogy and Geochemistry*, *48*(1), 391–425. doi: 10.2138/rmg.2002.48.10

Gabet, E. J., & Mudd, S. M. (2009). A theoretical model coupling chemical weathering rates with denudation rates. *Geology*, *37*(2), 151–154. doi: 10.1130/G25270A.1

Gaillardet, J., Dupré, B., Louvat, P., & Allègre, C. J. (1999). Global silicate weathering and CO_2 consumption rates deduced from the chemistry of large rivers. *Chemical Geology*, *159*(1-4), 3–30. doi: 10.1016/S0009-2541(99)00031-5

Galy, V., Peucker-Ehrenbrink, B., & Eglinton, T. (2015). Global carbon export from the terrestrial biosphere controlled by erosion. *Nature*, *521*(7551), 204–207. doi: 10.1038/nature14400

Gehman, H. M. (1962). Organic matter in limestones. *Geochimica et Cosmochimica Acta*, *26*(8), 885–897. doi: 10.1016/0016-7037(62)90118-7

Goddéris, Y., & Donnadieu, Y. (2019). A sink- or a source-driven carbon cycle at the geological timescale? Relative importance of palaeogeography versus solid Earth degassing rate in the Phanerozoic climatic evolution. *Geological Magazine*, *156*(2), 355–365. doi: 10.1017/S0016756817001054

Goddéris, Y., & Joachimski, M. M. (2004). Global change in the Late Devonian: modelling the Frasnian–Famennian short-term carbon isotope excursions. *Palaeogeography, Palaeoclimatology, Palaeoecology*, *202*(3-4), 309–329. doi: 10.1016/S0031-0182(03)00641-2

Gwiazda, R. H., & Broecker, W. S. (1994). The separate and combined effects of temperature, soil pCO_2, and organic acidity on silicate weathering in the soil environment: Formulation of a model and results. *Global Biogeochemical Cycles*, *8*(2), 141–155. doi: 10.1029/94GB00491

Hartmann, J., & Moosdorf, N. (2012). The new global lithological map database GLiM: A representation of rock properties at the Earth surface. *Geochemistry, Geophysics, Geosystems*, *13*(12). doi: 10.1029/2012GC004370

Hartmann, J., Moosdorf, N., Lauerwald, R., Hinderer, M., & West, A. J. (2014). Global chemical weathering and associated P-release — The role of lithology, temperature and soil properties. *Chemical Geology*, *363*, 145–163. doi: 10.1016/j.chemgeo.2013.10.025

Hartnett, H. E., Keil, R. G., Hedges, J. I., & Devol, A. H. (1998). Influence of oxygen exposure time on organic carbon preservation in continental margin sediments. *Nature*, *391*(6667), 572–575. doi: 10.1038/35351

Hilton, R. G., Gaillardet, J., Calmels, D., & Birck, J.-L. (2014). Geological respiration of a mountain belt revealed by the trace element rhenium. *Earth and Planetary Science Letters*, *403*, 27–36. doi: 10.1016/j.epsl.2014.06.021

Hilton, R. G., & West, A. J. (2020). Mountains, erosion and the carbon cycle. *Nature Reviews Earth & Environment*, *1*(6), 284–299. doi: 10.1038/s43017-020-0058-6

Kurtz, A. C., Kump, L. R., Arthur, M. A., Zachos, J. C., & Paytan, A. (2003). Early Cenozoic decoupling of the global carbon and sulfur cycles. *Paleoceanography*, *18*(4). doi: 10.1029/2003PA000908

Kölling, M., Bouimetarhan, I., Bowles, M. W., Felis, T., Goldhammer, T., Hinrichs, K.-U., ... Zabel, M. (2019). Consistent CO_2 release by pyrite oxidation on continental shelves prior to glacial terminations. *Nature Geoscience*, *12*(11), 929–934. doi: 10.1038/s41561-019-0465-9

Lenton, T. M., Daines, S. J., & Mills, B. J. (2018). COPSE reloaded: An improved model of biogeochemical cycling over Phanerozoic time. *Earth-Science Reviews*, *178*, 1–28. doi: 10.1016/j.earscirev.2017.12.004

Lenton, T. M., & Watson, A. J. (2000). Redfield revisited: 2. What regulates the oxygen content of the atmosphere? *Global Biogeochemical Cycles*, *14*(1), 249–268. doi: 10.1029/1999GB900076

Lieth, H. (1984). Biomass pools and primary produetivity of natural and managed ecosystem types in a global perspective. *Workshop agroecology. Paris : CIHEAM, 1984 (Options Méditerranéennes : Série Etudes)*, *1984-I*, 7–14. Retrieved from `http://om.ciheam.org/om/pdf/s07/CI010834.pdf`

Maffre, P., Ladant, J.-B., Donnadieu, Y., Sepulchre, P., & Goddéris, Y. (2018). The influence of orography on modern ocean circulation. *Climate Dynamics*, *50*(3-4), 1277–1289. doi: 10.1007/s00382-017-3683-0

Maffre, P., Ladant, J.-B., Moquet, J.-S., Carretier, S., Labat, D., & Goddéris, Y. (2018). Mountain ranges, climate and weathering. Do orogens strengthen or weaken the silicate weathering carbon sink? *Earth and Planetary Science Letters*, *493*, 174–185. doi: 10.1016/j.epsl.2018.04.034

Mills, B. J., Belcher, C. M., Lenton, T. M., & Newton, R. J. (2016). A modeling case for high atmospheric oxygen concentrations during the Mesozoic and Cenozoic. *Geology*, *44*(12), 1023–1026. doi: 10.1130/G38231.1

Muñoz Sabater, J. (2019). *ERA5-Land monthly averaged data from 2001 to present.* Copernicus Climate Change Service (C3S) Climate Data Store (CDS), ECMWF. Retrieved 2020-02-19, from `https://cds.climate.copernicus.eu/doi/10.24381/cds.68d2bb30` (type: dataset) doi: 10.24381/CDS.68D2BB30

Park, Y., Maffre, P., Goddéris, Y., Macdonald, F. A., Anttila, E. S. C., & Swanson-Hysell, N. L. (2020). Emergence of the Southeast Asian islands as a driver for Neogene cooling. *Proceedings of the National Academy of Sciences*, *117*(41), 25319–25326. doi: 10.1073/pnas.2011033117

Raiswell, R., & Berner, R. A. (1986). Pyrite and organic matter in Phanerozoic normal marine shales. *Geochimica et Cosmochimica Acta*, *50*(9), 1967–1976. doi: 10.1016/0016-7037(86)90252-8

Shields, G. A., & Mills, B. J. W. (2021, March). Evaporite weathering and deposition as a long-term climate forcing mechanism. *Geology*, *49*(3), 299–303. doi: 10.1130/G48146.1

Shukla, T., Sundriyal, S., Stachnik, L., & Mehta, M. (2018). Carbonate and silicate weathering in glacial environments and its relation to atmospheric CO_2 cycling in the Himalaya. *Annals of Glaciology*, *59*(77), 159–170. doi: 10.1017/aog.2019.5

Simon, L., Goddéris, Y., Buggisch, W., Strauss, H., & Joachimski, M. M. (2007). Modeling the carbon and sulfur isotope compositions of marine sediments: Climate evolution during the Devonian. *Chemical Geology*, *246*(1-2), 19–38. doi: 10.1016/j.chemgeo.2007.08.014

Spence, J., & Telmer, K. (2005). The role of sulfur in chemical weathering and atmospheric CO_2 fluxes: Evidence from major ions, $\delta^{13}C_{DIC}$, and $\delta^{34}S_{SO4}$ in rivers of the Canadian Cordillera. *Geochimica et Cosmochimica Acta*, *69*(23), 5441–5458. doi: 10.1016/j.gca.2005.07.011

Torres, M. A., Moosdorf, N., Hartmann, J., Adkins, J. F., & West, A. J. (2017). Glacial weathering, sulfide oxidation, and global carbon cycle feedbacks. *Proceedings of the National Academy of Sciences*, *114*(33), 8716–8721. doi: 10.1073/pnas.1702953114

Torres, M. A., West, A. J., Clark, K. E., Paris, G., Bouchez, J., Ponton, C., ... Adkins, J. F. (2016). The acid and alkalinity budgets of weathering in the Andes–Amazon system: Insights into the erosional control of global biogeochemical cycles. *Earth and Planetary Science Letters*, *450*, 381–391. doi: 10.1016/j.epsl.2016.06.012

Torres, M. A., West, A. J., & Li, G. (2014). Sulphide oxidation and carbonate dissolution as a source of CO_2 over geological timescales. *Nature*, *507*(7492), 346–349. doi: 10.1038/nature13030

Van Cappellen, P., & Ingall, E. D. (1994). Benthic phosphorus regeneration, net primary production, and ocean anoxia: A model of the coupled marine biogeochemical cycles of carbon and phosphorus. *Paleoceanography*, *9*(5), 677–692. doi: 10.1029/94PA01455

Van Cappellen, P., & Ingall, E. D. (1996). Redox Stabilization of the Atmosphere and Oceans by Phosphorus-Limited Marine Productivity. *Science*, *271*(5248), 493–496. doi: 10.1126/science.271.5248.493

Walker, J. C. G., Hays, P. B., & Kasting, J. F. (1981). A negative feedback mechanism for the long-term stabilization of Earth's surface temperature. *Journal of Geophysical Research*, *86*(C10), 9776. doi: 10.1029/JC086iC10p09776

West, A. J. (2012). Thickness of the chemical weathering zone and implications for erosional and climatic drivers of weathering and for carbon-cycle feedbacks. *Geology*, *40*(9), 811–814. doi: 10.1130/G33041.1

Wheat, C. G., Feely, R. A., & Mottl, M. J. (1996, October). Phosphate removal by oceanic hydrothermal processes: An update of the phosphorus budget in the oceans. *Geochimica et Cosmochimica Acta*, *60*(19), 3593–3608. doi: 10.1016/0016-7037(96)00189-5

Supporting Information for "Limited Carbon Cycle Response to Increased Sulfide Weathering due to Oxygen Feedback"

Pierre Maffre[1], Nicholas Swanson-Hysell[1], Yves Goddéris[2]

[1]University of California, Berkeley, department of Earth and Planetary Sciences

[2]Géosciences Environnement Toulouse, CNRS—Université Paul Sabatier - IRD, 31400 Toulouse, France.

Contents of this file

1. Text S1 to S5
2. Figures S1 to S10
3. Tables S1 to S3

Introduction

This document provides additional information on the numerical model used for the simulations presented, as well as the calibration procedure of the model, and its parameterization.

It also contains additional numerical simulations that were conducted for this study.

Text S1. Model description — continental weathering

The continental weathering module of GEOCLIM computes the following spatially-resolved values (for the present study, the resolution is 0.5°×0.5°):

1. E: Physical erosion (m/a)
2. F_{sw}: Silicate weathering (mol/m^2/a)
3. F_{cw}: Carbonate weathering (mol/m^2/a)
4. F_{kw}: Kerogen weathering (mol/m^2/a)
5. F_{sulf}: Sulfide weathering (mol/m^2/a)
6. F_{ocx}: Terrestrial organic carbon export (mol/m^2/a)
7. F_{pw}: Phosphorus weathering (mol/m^2/a)

The following variables set these fluxes:

- T: Surface temperature, at current CO_2 level (K)
- q: Total runoff, i.e, precipitation minus evaporation, at current CO_2 level (m/a)
- S: Slope of the land (m/m)
- $x_L(i)$: Area fraction of grid cell covered by the lithological class $\#i$

Temperature and runoff are annual-mean climatological averages (e.g., average over 30 years of equilibrium climate). Slope was computed as the gradient of elevation using the SRTM digital elevation model at 30 seconds resolution, and then averaged at 0.5°. Lithology fractions on each 0.5° grid cell was derived from the shapefile of Hartmann and Moosdorf (2012).

The lithological classes used are:

1. Metamorphic

2. Mafic and ultramafic

3. Intermediate

4. Felsic

5. Siliclastic sediments

6. Carbonate

Erosion:

The equation for erosion rate is derived from the Stream Power Incision Model (Davy & Crave, 2000) and adapted for a regular longitude-latitude grid (Maffre et al., 2018):

$$E \;=\; k_e\, q^{0.5}\, S \tag{1}$$

Where k_e is the erodibility constant.

Silicate Weathering:

Silicate weathering is computed using the regolith model of Gabet and Mudd (2009), with the parameterization of West (2012). We consider the "regolith" as the interface between unweathered bedrock and earth surface, where chemical weathering reactions occur. The regolith model describes a vertical profile of abundance of primary minerals, starting from 1 at regolith/bedrock transition, and decaying towards the surface due to dissolution reactions.

Regolith thickness h is computed as:

$$\frac{dh}{dt} \;=\; P_o f(h) - E \tag{2}$$

Where P_o is the optimal regolith production rate, computed as:

$$P_o \;=\; k_{rp}\, q\, e^{-\frac{E_{Arp}}{R}\left(\frac{1}{T}-\frac{1}{T_o}\right)} \tag{3}$$

Where R is the ideal gas constant, T_o the chosen reference temperature (288.15 K), E_{Arp} the apparent activation energy at T_o for regolith production and k_{rp} the proportionality constant.

$f(h)$ is the soil production function, capturing the decrease of regolith production rate with a deeper bedrock/regolith transition. We considered an exponential form:

$$f(h) = e^{-h/h_o} \tag{4}$$

Where h_o is the decay depth.

The vertical profile of primary minerals x_p follows an advection-reaction equation (the downward migration of regolith/bedrock transition is equivalent to an upward advection of rock particles):

$$\begin{aligned} \frac{\partial x_z}{\partial t} &= -P_o f(h) \frac{\partial x_p}{\partial z} - K\tau^\sigma x_p \\ \frac{\partial \tau}{\partial t} &= -P_o f(h) \frac{\partial \tau}{\partial z} + 1 \end{aligned} \tag{5}$$

The vertical coordinate z varies from 0 at regolith/bedrock transition to h at surface (i.e., z is positive upward). τ is the "age" of rock particles at the local depth, that is the time elapsed since the particle have entered the regolith. $K\tau^\sigma$ can be seen as the dissolution rate constant (with an order-1 kinetics). The exponent σ describes the fact the rate constant decreases with the age of the particles. K is defined according to the equation:

$$K = k_d \left(1 - e^{-k_w q}\right) e^{-\frac{E_{Ad}}{R}\left(\frac{1}{T} - \frac{1}{T_o}\right)} \tag{6}$$

where k_w is the runoff saturation parameter, E_{Ad} the apparent activation energy at T_o for mineral dissolution, and k_d the dissolution constant.

Finally, the silicate weathering rate is the dissolution rate integrated over the regolith:

$$F_{sw}(i) = \chi_{\mathrm{CaMg}} \int_0^h K\,\tau^{\sigma}\,x_P\,.dz \tag{7}$$

Where χ_{CaMg} is the amount of calcium and magnesium per m^3 of bedrock (x_P is the fraction of primary minerals in the regolith normalized to the one of the bedrock, it does not describe the absolute amount of cations). Silicate weathering rate is then expressed in $\mathrm{mol(CaMg)/m^2/a}$.

The index (i) in equation 7 denotes that silicate weathering is computed for each silicate lithological class (5 are considered) given that parameters are lithology-dependent (see Table S1). The total silicate weathering rate is then:

$$F_{sw} = \sum_{i=1}^{N_{litho}} x_L(i) F_{sw}(i) \tag{8}$$

Carbonate weathering:

The carbonate weathering formulation used in the model has been slightly modified since Donnadieu et al. (2006). We used the formulations published in Arndt, Regnier, Goddéris, and Donnadieu (2011).

The $p\mathrm{CO_2}$ in the soil is computed as:

$$p\mathrm{CO_2}|_{soil} = p\mathrm{CO_2}|_{atm} + \frac{p\mathrm{CO_2}|_{soil}^{max}}{1 + e^{(1.315 - 0.116(T - 273.15))}} \tag{9}$$

(Gwiazda & Broecker, 1994). The maximum $p\mathrm{CO_2}$ in soil is defined as:

$$p\mathrm{CO_2}|_{soil}^{max} = 1 + 0.302484 q^{0.8} \tag{10}$$

(Lieth, 1984). q being here in cm/a.

That $p\mathrm{CO_2}$ in soil is then used to determine the equilibrium $\mathrm{Ca^{2+}}$ concentration with calcite and soil $\mathrm{CO_2}$ n ($[\mathrm{Ca^{2+}}]_{eq}$), and the carbonate weathering flux is computed assuming

dissolution kinetics are never limiting:

$$F_{cw} \;=\; k_{carb} \cdot x_L(i_{carb}) \cdot q \cdot [\mathrm{Ca}^{2+}]_{eq} \tag{11}$$

With $x_L(i_{carb})$ the fraction of the carbonate lithological class in the grid cell, and k_{carb} is a calibration constant (see Table S1).

Kerogen and sulfide weathering:

Kerogen weathering was updated with respect to published versions of GEOCLIM, and sulfide weathering is an addition of the present study.

Following (Calmels et al., 2007; Hilton et al., 2014), we assumed those fluxes to be proportional to the erosion rate:

$$F_{kw} = 0.5 \sum_{k=1}^{N_{litho}} x_L(k)\, \chi_{OC} E \tag{12}$$

$$F_{sulf} = \sum_{k=1}^{N_{litho}} x_L(k)\, \chi_{\mathrm{S}} E \tag{13}$$

Where χ_{OC} is the fraction of petrogenic organic carbon in bedrock, and χ_{S} is the amount of sulfur in the form of sulfide (e.g., FeS_2) in bedrock. The factor 0.5 for kerogen weathering accounts for the fact that only 50% of the petrogenic organic matter is considered as reactive (Hilton & West, 2020), the rest is taken to be inert and will not be oxidized at any point.

As stated in the main text, to determine the fraction of released sulfuric acid that dissolves carbonate mineral versus silicate mineral, we assumed that silicate:carbonate ratio to be the same as the ratio of total silicate and carbonate weathering flux by carbonic acid, as a neutral hypothesis. The total "carbonic weathering" fluxes are 4.7 Tmol/yr and

12.3 Tmol/yr, for silicate and carbonate (respectively). Hence, we assumed that 36.5% of the released sulfuric acid dissolves silicate minerals.

Terrestrial organic carbon export:

Terrestrial organic carbon export refers to the amount of organic carbon photosynthesized by the biosphere (i.e., produced from atmospheric CO_2) that is not respired, and is exported to the ocean by rivers in the form of particulate organic matter.

We used the formulation of (Galy et al., 2015), that is fit on field data:

$$F_{ocx} = \frac{1}{12}\, 0.081\, E^{0.56} \tag{14}$$

Where E is expressed in t/km^2/a (we assumed a density of 2500 kg/m^3). The factor 1/12 is for converting the flux in mol(C)/m^2/a.

Phosphorus weathering:

We updated the treatment of phosphorus weathering with respect to previously published versions of GEOCLIM. Phosphorus weathering is set proportional to the silicate, carbonate and kerogen weathering fluxes, with imposed concentration of non-organic P in source rocks, and C:P ratio in kerogen:

$$F_{pw} \;=\; \sum_{i=1}^{N_{litho}} \left(x_L(i) \frac{\chi_{\mathrm{P}}}{\chi_{\mathrm{CaMg}}} F_{sw}(i) \right) \;+\; \frac{\chi_{\mathrm{P}}(carb)}{\chi_{\mathrm{CaCO_3}}} F_{cw} \;+\; \frac{F_{kw}}{(\mathrm{C:P})_{ker}} \tag{15}$$

With χ_{P} the amount of phosphorus per m^3 of bedrock (lithology-dependent), $\chi_{\mathrm{CaCO_3}}$ is the amount of $CaCO_3$ per m^3 of carbonate, and $(\mathrm{C:P})_{ker}$ the ratio in kerogens.

Part of the weathered phosphorus is exported within the terrestrial organic carbon particles:

$$F^P_{part} \;=\; \frac{1}{(\mathrm{C:P})_{terr}} \iint_{land} F_{ocx}.dxdy \tag{16}$$

where $(C : P)_{terr}$ is the ratio of labile organic C and P in exported riverine particles. We assumed a ratio of 205 (on a molar basis), in order to get a realistic partition of phosphorus between particulate and dissolved form (Filippelli, 2002). All the remaining non-particular phosphorus is exported in dissolved form:

$$F^P_{diss} = \iint_{land} F_{pw}.dxdy - F^P_{part} \quad (17)$$

Text S2. Model description — oceanic deposition fluxes and early diagenesis module

The early diagenesis module of GEOCLIM computes the burial fluxes of the considered elements (organic and inorganic carbon, phosphorus, sulfur...). This module is similar from published version (Simon et al., 2007). We updated the calculation of sedimentation rate and the sulfate reduction part.

Sedimentation rate:

Originally, the sedimentation rate was imposed in different basin types of GEOCLIM: epicontinental surface (ES), epicontinental deep (ED), and deep open ocean (OD). In this updated version, the total sedimentation flux is computed, as the sum of riverine sediment delivery and oceanic particles deposited from the water column (carbonate precipitation and organic matter, these fluxes contribute to approximately 9% of the total flux). This sedimentation flux is then distributed in the different basins to compute their local sedimentation flux F^i_{sed} and sedimentation rate w^i_s.

The terrestrial sediments are delivered to the epicontinental surface basin. What is not deposited in this basin it is exported in the epicontinental deep basin, and what is not deposited in that second basin is exported to the open ocean deep basins (they are

actually 3 open deep basins). For each basin, the "imported" sediment flux (from previous basin or from land) is added to the flux of particles deposited from the water column F^i_{dep}. Hence:

$$\begin{aligned}
F^{ES}_{in} &= \rho_{tss} \iint_{land} E\,.dxdy \;+\; F^{ES}_{dep} \\
F^{ES}_{sed} &= \frac{F^{ES}_{in}}{1 \;+\; F^{ES}_{in}/C_{ES}} \\
F^{ED}_{in} &= F^{ES}_{in} \;-\; F^{ES}_{sed} \;+\; F^{ED}_{dep} \\
F^{ED}_{sed} &= \frac{F^{ED}_{in}}{1 \;+\; F^{ED}_{in}/C_{ED}} \\
F^{OD}_{sed} &= F^{ED}_{in} \;-\; F^{ED}_{sed} \;+\; F^{OD}_{dep}
\end{aligned} \tag{18}$$

Where ρ_{tss} is the density of riverine sediments (set to 2500 kg/m^3), F^i_{dep} is the total (mass) deposition flux of particles (PIC and POC) in the basin i, and C_i is the sedimentation capacity of the basin, which is the maximum sedimentation flux that a basin can have. It is defined as:

$$C_i = k_{sed}\,(A^i_s)^{3/2} \tag{19}$$

Where A^i_s is the seafloor area of the basin, and k_{sed} a calibration constant. Because they are 3 open deep basins, the input flux from the epicontinental deep basin is in fact split in those 3 basins proportionally to their seafloor area.

The sedimentation rate w^i_s of each basin i is then defined as:

$$w^i_s = \frac{F^i_{dep}}{\rho_{sed} A^i_s} \tag{20}$$

Where ρ_{sed} is the density of marine sediment, set to 2300 kg/m^3.

Early diagenesis and burial fluxes:

The burial fluxes in GEOCLIM are computed using an early diagenesis model, representing a bioturbated (mixed) sediment layer followed by sulfate reduction sediment layer (vertically). This module is described in (Simon et al., 2007), Appendix A. They are 2 main differences in the present study. 1. the sedimentation rate is not imposed, but calculated, and depends on the continental sediment delivery. 2. (Simon et al., 2007) used an inverse approach approach to quantify sulfate reduction from isotopic records, we used a forward modeling approach. The burial fluxes are computed as follows, for each "bottom" basin:

$$\begin{aligned} \mathrm{C}^{o} &= \frac{F^{\mathrm{C}}_{dep}}{F_{sed}/\rho_{sed}} \\ \mathrm{C}^{ml} &= \frac{w_s \mathrm{C}^{o}}{w_s + \beta\,[\mathrm{O}_2]\,h_{ml}} \\ \mathrm{C}^{srl} &= \frac{w_s \mathrm{C}^{ml}}{w_s + \gamma\,[{\mathrm{SO}_4}^{2-}]\,h_{srl}} \\ F_{ocb} &= \left(1 - x_{\mathrm{CH}_4}\right) w_s A_s \mathrm{C}^{srl} \\ F_{sr} &= \frac{1}{2} w_s A_s \left(\mathrm{C}^{ml} - \mathrm{C}^{srl}\right) \end{aligned} \tag{21}$$

where F^{C}_{dep} is the molar deposition flux of organic carbon, A_s the seafloor area, h^{ml} and h^{srl} the thickness of the mixed layer and the sulfate reduction layer (respectively). C^{o} is the concentration of organic carbon at the top of sediment, C^{ml} is the concentration at the bottom of the mixed layer, C^{srl} is the concentration at the bottom of the sulfate reduction layer. $[\mathrm{O}_2]$ and $[{\mathrm{SO}_4}^{2-}]$ are the concentration of oxygen and sulfate (respectively) in the local oceanic basin, used as proxy for concentration in sediment. β and γ are the reactions rate constants (i.e., the reaction rate is assumed to be proportional to the oxidant concentration times the organic carbon concentration). x_{CH_4} is the fraction of carbon loss in form of methane (that is thereafter reoxidized into CO_2 by O_2). Finally, F_{ocb} and F_{sr}

are, respectively, the local organic carbon burial flux and the sulfate reduction flux. The coefficient $\frac{1}{2}$ arises from the fact that for 2 C oxidized, 1 S is reduced.

The organic phosphorus burial flux F_{opb} is scaled to the organic carbon burial flux F_{ocb}, but with a different C:P ratio:

$$F_{opb} = \frac{F_{ocb}}{(\mathrm{C:P})_{burial}} \tag{22}$$

that ratio $(\mathrm{C:P})_{burial}$ is parameterized with the degree of anoxicity DOA:

$$(\mathrm{C:P})_{burial} = \frac{(\mathrm{C:P})_{oxic} \cdot (\mathrm{C:P})_{anoxic}}{(1 - DOA) \cdot (\mathrm{C:P})_{anoxic} + DOA \cdot (\mathrm{C:P})_{oxic}} \tag{23}$$

In other words, the amount of P buried for a given amount of buried C varies linearly with the DOA between the 2 end-members.

The DOA qualitatively represents the fraction of the basin that is anoxic. It varies from 1 (fully anoxic basin) to 0 (fully oxic basin). It only depends on local oxygen concentration, using the relation of Van Cappellen and Ingall (1994, polynomial fit of Figure 4A of their contribution). Roughly speaking, it linearly decreases from 1 for $[O_2] = 0$ mol/m^3 to 0 for $[O_2] = 0.4$ mol/m^3 (see Figure S1).

The end-member burial C:P ratio are $(\mathrm{C:P})_{oxic} = 200$ and $(\mathrm{C:P})_{anoxic} = 4000$. This provides an negative feedback for oxygen, for as oxygen level decreases, less phosphorus is buried with organic carbon, which makes more phosphorus available at surface (through upwellings), which increases the primary productivity, and hence the production of O_2. This accumulation of O_2 dissolved in seawater counteracts the spreading of anoxic conditions, and consequently limits the burial of organic carbon.

The particulate organic C and P deposited but not buried are converted into dissolved form in the local basin (and will be advected by the ocean circulation).

Two additional sinks of phosphorus are considered: hydrothermal burial F_{phyd} , and burial in form of phosphorite F_{pbur}, both of them are proportional to the dissolved phosphorus concentration in deep basins:

$$F_{phyd} = k_{phyd}[\mathrm{P}]_{diss} \tag{24}$$

$$F_{pbur} = k_{pbur}[\mathrm{P}]_{diss} \tag{25}$$

Particulate inorganic carbon (PIC) deposited on seafloor are entirely preserved and buried. The early diagenesis only affects particulate organic carbon and phosphorus.

Text S3. Calibration and Initial Steady-State

The model was calibrated to reproduce pre-industrial conditions using ERA5 reanalysis of temperature and runoff (Muñoz Sabater, J., 2019) and modern fields of slope and lithology, under the assumption of steady-state. A second calibration was conducted with the climate fields from GFDL climate model at $1 \times CO_2$. Only a few parameters were adjusted for that second calibration (see Table S1). This last parameterization and pre-industrial steady-state are the ones used for all the simulations presented in this study.

ERA5-calibration:

We used the best-fit silicate weathering parameters of Park et al. (2020, presented in their SI), that calibrated the model with riverine data. That study used the same lithology classification and field of lithology fraction (Hartmann & Moosdorf, 2012). It yields a total silicate weathering flux of 4.70 Tmol(CaMg)/yr.

The carbonate weathering proportionality constant k_{carb} (eq. 11) was tuned to get a total carbonate weathering flux of 12.3 Tmol(C)/yr (Gaillardet et al., 1999).

Regarding the amount of organic carbon in rocks, we considered the value of Gehman (1962) for carbonate, and we tuned the organic carbon amount in siliclastic sediments to achieve a total flux of 5 Tmol(C)/yr (Lenton et al., 2018). We also assumed in eq. 12 that only half of the organic carbon is reactive for oxidation. (Hilton & West, 2020).

We considered a constant C:S ratio (7.69) to get a total sulfide weathering flux of 1.3 Tmol(S)/yr (Burke et al., 2018). This ratio is also consistent with observed ones in modern marine sediment and quaternay shales (Berner & Raiswell, 1983; Raiswell & Berner, 1986; Kurtz et al., 2003).

We used the parameterization of Galy et al. (2015) for terrestrial organic carbon export, without any modification. It yields a total flux of 10.5 Tmol(C)/yr.

We considered the amount of phosphorus in bedrock (lithology-dependent, including carbonate) from Hartmann, Moosdorf, Lauerwald, Hinderer, and West (2014). However, because it generated total P weathering flux that was too high, we chose to reduce the amount of P in siliclastic sediment (see Table S1). Regarding the amount of P in kerogen, we considered a C:P ratio of 500. This yields a global phosphorus weathering flux of 97.4 Gmol/yr. 51.2 Gmol/yr of that flux is exported bounded to terrestrial organic carbon particles, the remaining 46.2 Gmol/yr is exported in dissolved form.

We then imposed a CO_2 degassing from solid Earth that balances the silicate weathering Ca-Mg flux from both weathering from both atmospheric CO_2 (carbonic acid) and sulfide weathering generated H_2SO_4, that is 5.06 Tmol/yr.

The sedimentation capacity parameter k_{sed} (eq. 19) was tuned to get a realistic sedimentation rate contrast between the epicontinental basins and the deep open-ocean basins (0.7 mm/yr in epicontinental surface basin, 0.3 mm/yr in epicontinental deep basin, and $4 \cdot 10^{-4} - 3 \cdot 10^{-3}$ mm/yr in open-ocean deep basins). This is consistent with previously published versions of GEOCLIM. See also Table S2.

The constants k_{phyd} (eq. 24) and k_{pbur} (eq. 25), controlling "inorganic" phosphorus burial, were tuned in order for the primary productivity to generate realistic oxygen profiles, with a minimum of O_2 in the mid-lat thermocline basin. Indeed, an inorganic P burial not efficient enough would generate high oceanic P concentration, leading to high primary productivity (via P upwelling) and deep ocean anoxia. On the opposite,

too efficient inorganic P burial would result in not enough primary productivity and too high oxygen concentration in intermediate waters. The phosphorus burial fluxes are 13.2 Gmol/yr with organic matter, 15.0 Gmol/yr hydrothermal, and 69.2 Gmol/yr in form of phosphorite.

Regarding the early diagenesis module, the rate constant for organic carbon oxidation in bioturbated layer, β, and sulfate reduction, γ (eq. 21) were tuned so that the burial fluxes balance the continental oxidative weathering fluxes for pre-industrial atmospheric O_2 levels and mean oceanic ${SO_4}^{2-}$ (respectively, 21 % of atmosphere volume, and 29 mol/m^3 of mean oceanic sulfate concentration).

GFDL-calibration:

When switching from ERA5 climate fields to the GFDL model results, no modification was made for silicate and carbonate weathering, though the fluxes are lower (3.80 Tmol/yr and 7.81 Tmol/yr, respectively). However, the prescribed amount of organic carbon have been adjusted to keep the same kerogen and sulfide weathering fluxes (see Table S2). The phosphorus amount in siliclastic sediments was also adjusted to compensate for the lower silicate and carbonate weathering flux and keep the same phosphorus weathering flux. Because the global erosion flux (and then oceanic sedimentation flux) is also lower with GFDL fields, we adjusted the early diagenesis parameters β and γ in order to balance oxygen and sulfur cycle at the same pre-industrial pO_2 and ${SO_4}^{2-}$ concentration. Finally, the CO_2 degassing was reset to 4.16 Tmol/yr to balance sulfuric and carbonic silicate weathering.

The values of all parameters, for both ERA5 and GFDL calibration, are shown in Tables S1 and S2.

Text S4. Design of oxygen feedback sensitivity experiments

We modified the strength of the GEOCLIM oxygen feedback by adding or removing O_2 dependencies to some processes.

In the reference case ("reference"), two processes are responsible for the oxygen negative feedback: the diagenetic oxidation of deposited organic carbon in the bioturbated layer of marine sediment (eq. 21) and the C:P burial ratio that increases with anoxia (eq. 23), leading to enhance bioproductivity, and thus organic carbon burial.

To strengthen the oxygen feedback, we added a O_2-dependency to the hydrothermal P burial, by modifying eq. 24:

$$F_{phyd} \;=\; k'_{phyd}\,[\mathrm{P}]_{diss}\,[\mathrm{O_2}]_{diss} \tag{26}$$

for the "feedback+1" case.

And a stronger dependency for the "feedback+2" case:

$$F_{phyd} \;=\; k''_{phyd}\,[\mathrm{P}]_{diss}\,\left([\mathrm{O_2}]_{diss}\right)^2 \tag{27}$$

k'_{phyd} and k''_{phyd} were adjusted so that the equilibrium $p\mathrm{O_2}$ stays at 1 PAL.

Case "feedback+3" was built by further adding an O_2-dependency to terrestrial organic carbon export (eq. 14):

$$F_{ocx} \;=\; \frac{1}{12}\,0.081\,E^{0.56}\,/\,\left(p\mathrm{O_2}\right)^{1/2} \tag{28}$$

And a stronger dependency for "feedback+4":

$$F_{ocx} \;=\; \frac{1}{12}\,0.081\,E^{0.56}\,/\,p\mathrm{O_2} \tag{29}$$

$p\mathrm{O_2}$ begin expressed in PAL.

To reduce oxygen feedback, we set the degree of anoxicity (DOA) constant at 0.495 to remove the P-based oxygen feedback (case "feedback-1"). This value allows equilibrium $p\mathrm{O}_2$ to stay at 1 PAL.

For the case "feedback-2", we further added a reduced O_2-dependency to diagenetic organic carbon oxidation by modifying eq. 21:

$$\mathrm{C}^{ml} = \frac{w_s \mathrm{C}^o}{w_s + \beta \left(0.234\,[\mathrm{O}_2]\right)^{1/2} h_{ml}} \tag{30}$$

The factor 0.234, with dimension $\mathrm{mol/m^3}$, is here to make the equilibrium $p\mathrm{O}_2$ stay at 1 PAL.

Finally, for the "no-feedback" case, we removed that last O_2 dependency (still in eq. 21):

$$\mathrm{C}^{ml} = \frac{w_s \mathrm{C}^o}{w_s + \beta\, 0.23406\, h_{ml}} \tag{31}$$

The factor 0.23406, with dimension $\mathrm{mol/m^3}$, was tuned to minimize the oxygen drift with pre-industrial forcings and other geochemical species at equilibrium. Indeed, without any process dependent on oxygen (with the exception of water column remineralization under oxygen concentration lower than 8 $\mathrm{mmol/m^3}$), there is no equilibrium $p\mathrm{O}_2$ strictly speaking. With this parameterization, the $p\mathrm{O}_2$ drift is about $1.6 \cdot 10^{-5}$ PAL/Myr, which is negligible with respect to the perturbations we applied in our experiments.

The design of those seven cases is summarized in Table S3 and Figure S2.

Text S5. Additional experiments

Fates of sulfuric acid from sulfide oxidation:

We repeated the "abrupt" sulfide weathering perturbation experiment with different end-member scenarios for the additional sulfuric acid released by the perturbation:

- "H_2SO_4 release": leaching of H_2SO_4 in rivers (handled as negative alkalinity flux to the ocean)
- "Silicate trade-off": dissolution of silicate minerals compensated by an equal decrease of silicate weathering by carbonic acid.
- "Carbonate trade-off": dissolution of carbonate minerals compensated by an equal decrease of carbonate weathering by carbonic acid.

The results of these experiments are presented in Figures S4, S5, S6, S7 and S8. The geochemical species evolutions are almost identical to the "Carbonate" scenario (discussed in the main text). The only differences concerned the absolute fluxes, but the net fluxes (sources minus sinks) are virtually unchanged.

Joint perturbation of kerogen and sulfide oxidative weathering:

We considered here a proportional (abrupt) perturbation of kerogen weathering and sulfide weathering (with additional H_2SO_4 dissolving carbonate minerals) that have the same initial net carbon flux. In other words, instead of increasing by 50% the sulfide weathering flux, we increased by 10.32% the kerogen weathering and sulfide weathering fluxes. We tested 2 cases: one where the phosphorus weathering flux follows the increase of kerogen weathering (owing to the (C:P) ratio in kerogens), "Carb, sulf & ker – P", and

one where phosphorus weathering is unchanged, "Carb, sulf & ker – no P". The results of these experiments are presented in Figure S9.

Carbonate-sulfide perturbation with fixed temperature:

We repeated here the reference "carbonate" abrupt sulfide weathering perturbation (+50% of sulfide weathering, dissolving carbonate minerals) while artificially keeping constant (at pre-industrial level) either just oceanic temperature, or the entire climate (CO_2, temperature and runoff). Keeping oceanic temperature constant allows to evaluate the effect of temperature-dependent O_2 solubility for the organic carbon cycle feedbacks. Holding a constant CO_2 level keeps all the continental weathering fluxes at their initial values (except for the sulfide weathering perturbation), and provides an alternative way to determine when the sulfide perturbation transitions from a source to a sink of carbon. The results of these experiments are presented in Figure S10.

References

Arndt, S., Regnier, P., Goddéris, Y., & Donnadieu, Y. (2011). GEOCLIM reloaded (v 1.0): a new coupled earth system model for past climate change. *Geoscientific Model Development*, *4*(2), 451–481. doi: 10.5194/gmd-4-451-2011

Berner, R. A., & Raiswell, R. (1983). Burial of organic carbon and pyrite sulfur in sediments over Phanerozoic time: a new theory. *Geochimica et Cosmochimica Acta*, *47*(5), 855–862. doi: 10.1016/0016-7037(83)90151-5

Burke, A., Present, T. M., Paris, G., Rae, E. C., Sandilands, B. H., Gaillardet, J., ... Adkins, J. F. (2018). Sulfur isotopes in rivers: Insights into global weathering budgets, pyrite oxidation, and the modern sulfur cycle. *Earth and Planetary Science*

Letters, *496*, 168–177. doi: 10.1016/j.epsl.2018.05.022

Calmels, D., Gaillardet, J., Brenot, A., & France-Lanord, C. (2007). Sustained sulfide oxidation by physical erosion processes in the Mackenzie River basin: Climatic perspectives. *Geology*, *35*(11), 1003. doi: 10.1130/G24132A.1

Davy, P., & Crave, A. (2000). Upscaling local-scale transport processes in large-scale relief dynamics. *Physics and Chemistry of the Earth, Part A: Solid Earth and Geodesy*, *25*(6-7), 533–541. doi: 10.1016/S1464-1895(00)00082-X

Donnadieu, Y., Goddéris, Y., Pierrehumbert, R., Dromart, G., Fluteau, F., & Jacob, R. (2006). A GEOCLIM simulation of climatic and biogeochemical consequences of Pangea breakup. *Geochemistry, Geophysics, Geosystems*, *7*(11). doi: 10.1029/2006GC001278

Filippelli, G. M. (2002). The Global Phosphorus Cycle. *Reviews in Mineralogy and Geochemistry*, *48*(1), 391–425. doi: 10.2138/rmg.2002.48.10

Gabet, E. J., & Mudd, S. M. (2009). A theoretical model coupling chemical weathering rates with denudation rates. *Geology*, *37*(2), 151–154. doi: 10.1130/G25270A.1

Gaillardet, J., Dupré, B., Louvat, P., & Allègre, C. J. (1999). Global silicate weathering and CO_2 consumption rates deduced from the chemistry of large rivers. *Chemical Geology*, *159*(1-4), 3–30. doi: 10.1016/S0009-2541(99)00031-5

Galy, V., Peucker-Ehrenbrink, B., & Eglinton, T. (2015). Global carbon export from the terrestrial biosphere controlled by erosion. *Nature*, *521*(7551), 204–207. doi: 10.1038/nature14400

Gehman, H. M. (1962). Organic matter in limestones. *Geochimica et Cosmochimica*

Acta, *26*(8), 885–897. doi: 10.1016/0016-7037(62)90118-7

Gwiazda, R. H., & Broecker, W. S. (1994). The separate and combined effects of temperature, soil pCO_2, and organic acidity on silicate weathering in the soil environment: Formulation of a model and results. *Global Biogeochemical Cycles*, *8*(2), 141–155. doi: 10.1029/94GB00491

Hartmann, J., & Moosdorf, N. (2012). The new global lithological map database GLiM: A representation of rock properties at the Earth surface. *Geochemistry, Geophysics, Geosystems*, *13*(12). doi: 10.1029/2012GC004370

Hartmann, J., Moosdorf, N., Lauerwald, R., Hinderer, M., & West, A. J. (2014). Global chemical weathering and associated P-release — The role of lithology, temperature and soil properties. *Chemical Geology*, *363*, 145–163. doi: 10.1016/j.chemgeo.2013.10.025

Hilton, R. G., Gaillardet, J., Calmels, D., & Birck, J.-L. (2014). Geological respiration of a mountain belt revealed by the trace element rhenium. *Earth and Planetary Science Letters*, *403*, 27–36. doi: 10.1016/j.epsl.2014.06.021

Hilton, R. G., & West, A. J. (2020). Mountains, erosion and the carbon cycle. *Nature Reviews Earth & Environment*, *1*(6), 284–299. doi: 10.1038/s43017-020-0058-6

Kurtz, A. C., Kump, L. R., Arthur, M. A., Zachos, J. C., & Paytan, A. (2003). Early Cenozoic decoupling of the global carbon and sulfur cycles. *Paleoceanography*, *18*(4). doi: 10.1029/2003PA000908

Lenton, T. M., Daines, S. J., & Mills, B. J. (2018). COPSE reloaded: An improved model of biogeochemical cycling over Phanerozoic time. *Earth-Science Reviews*, *178*, 1–28.

doi: 10.1016/j.earscirev.2017.12.004

Lieth, H. (1984). Biomass pools and primary produetivity of natural and managed ecosystem types in a global perspective. *Workshop agroecology. Paris : CIHEAM, 1984 (Options Méditerranéennes : Série Etudes)*, *1984-I*, 7–14. Retrieved from http://om.ciheam.org/om/pdf/s07/CI010834.pdf

Maffre, P., Ladant, J.-B., Moquet, J.-S., Carretier, S., Labat, D., & Goddéris, Y. (2018). Mountain ranges, climate and weathering. Do orogens strengthen or weaken the silicate weathering carbon sink? *Earth and Planetary Science Letters*, *493*, 174–185. doi: 10.1016/j.epsl.2018.04.034

Muñoz Sabater, J. (2019). *ERA5-Land monthly averaged data from 2001 to present.* Copernicus Climate Change Service (C3S) Climate Data Store (CDS), ECMWF. Retrieved 2020-02-19, from https://cds.climate.copernicus.eu/doi/10.24381/cds.68d2bb30 (type: dataset) doi: 10.24381/CDS.68D2BB30

Park, Y., Maffre, P., Goddéris, Y., Macdonald, F. A., Anttila, E. S. C., & Swanson-Hysell, N. L. (2020). Emergence of the Southeast Asian islands as a driver for Neogene cooling. *Proceedings of the National Academy of Sciences*, *117*(41), 25319–25326. doi: 10.1073/pnas.2011033117

Raiswell, R., & Berner, R. A. (1986). Pyrite and organic matter in Phanerozoic normal marine shales. *Geochimica et Cosmochimica Acta*, *50*(9), 1967–1976. doi: 10.1016/0016-7037(86)90252-8

Simon, L., Goddéris, Y., Buggisch, W., Strauss, H., & Joachimski, M. M. (2007). Modeling the carbon and sulfur isotope compositions of marine sediments: Cli-

mate evolution during the Devonian. *Chemical Geology*, *246*(1-2), 19–38. doi: 10.1016/j.chemgeo.2007.08.014

Van Cappellen, P., & Ingall, E. D. (1994). Benthic phosphorus regeneration, net primary production, and ocean anoxia: A model of the coupled marine biogeochemical cycles of carbon and phosphorus. *Paleoceanography*, *9*(5), 677–692. doi: 10.1029/94PA01455

West, A. J. (2012). Thickness of the chemical weathering zone and implications for erosional and climatic drivers of weathering and for carbon-cycle feedbacks. *Geology*, *40*(9), 811–814. doi: 10.1130/G33041.1

Table S1. Continental parameters

Parameter	Eq.	units	values (per lithology)					
			metam.	felsic	interm.	mafic	sil. sed.	carb.
k_e	1	$m^{0.5}a^{-0.5}$	$3.0713 \cdot 10^{-3}$					
T_o	3,6	K	286					-
k_{rp}	3	-	$1 \cdot 10^{-2}$					-
E_{Arp}	3	J/mol/K	42000					-
h_o	4	m	2.73					-
σ	5	-	-0.4					-
k_d	6	$a^{-1-\sigma}$	$5 \cdot 10^{-4}$					-
k_w	6	$m^{-1}a$	1					-
E_{Ad}	6	J/mol/K	42000					-
χ_{CaMg}	7	mol/m^3	2500	1521	4759	10317	2000	0
k_{carb}	11	-	-					3.589
χ_{OC}	12	mol/m^3	0	0	0	0	2562.5[a], 3023.96[b]	500
χ_{S}	13	mol/m^3	$\chi_{OC}/7.68$					
χ_{P}	15	mol/m^3	63.76	49.60	168.2	121.3[a], 338.0[b]	4 (41.97[c])	38.08
$\chi_{\mathrm{CaCO_3}}$	15	mol/m^3	-					25000
$(\mathrm{C:P})_{ker}$	15	mol/mol	500					
$(\mathrm{C:P})_{terr}$	17	mol/mol	205					

[a]ERA5-calibration, [b]GFDL-calibration, [c](Hartmann et al., 2014) value

Table S2. Oceanic parameters

Parameter	ρ_{tss}	k_{sed}	ρ_{sed}		
Equations	18	19	20, 21		
units	kg/m^3	a^{-1}	kg/m^3		
value	2500	$2 \cdot 10^{-9}$	2300		
Parameter	β	h_{ml}	γ	h_{srl}	x_{CH_4}
Equations	21	21	21	21	21
units	$mol^{-1}m^3a^{-1}$	m	$mol^{-1}m^3a^{-1}$	m	-
value	$6.4602 \cdot 10^{-2}$[a]	0.05	$1.6292 \cdot 10^{-5}$[a]	0.5	0.36
	$5.4245 \cdot 10^{-2}$[b]		$1.38596 \cdot 10^{-5}$[b]		
Parameter	$(C:P)_{oxic}$	$(C:P)_{anoxic}$	k_{phyd}	k_{pbur}	
Equation	23	23	24	25	
units	mol/mol	mol/mol	m^3a^{-1}	m^3a^{-1}	
value	200	4000	$2.166 \cdot 10^{12}$	$1 \cdot 10^{13}$	

[a]ERA5-calibration, [b]GFDL-calibration

Table S3. Oxygen feedback cases

name	sed org C oxid	DOA	hydr P bur	terr bio C exp	eq O_2 level (PAL)	
					control	+50% ker wth
no-feedback	indep. of O_2	constant	indep. of O_2	indep. of O_2	(~ 1)	-
feedback-2	$\propto [O_2]^{0.5}$	constant	indep. of O_2	indep. of O_2	1.00	0.44
feedback-1	$\propto [O_2]$	constant	indep. of O_2	indep. of O_2	1.00	0.51
reference	$\propto [O_2]$	$f([O_2])$	indep. of O_2	indep. of O_2	1.00	0.56
feedback+1	$\propto [O_2]$	$f([O_2])$	$\propto [O_2]$	indep. of O_2	1.00	0.61
feedback+2	$\propto [O_2]$	$f([O_2])$	$\propto [O_2]^2$	indep. of O_2	1.00	0.63
feedback+3	$\propto [O_2]$	$f([O_2])$	$\propto [O_2]^2$	$\propto (p_{O_2})^{-0.5}$	1.00	0.65
feedback+4	$\propto [O_2]$	$f([O_2])$	$\propto [O_2]^2$	$\propto (p_{O_2})^{-1}$	1.00	0.68

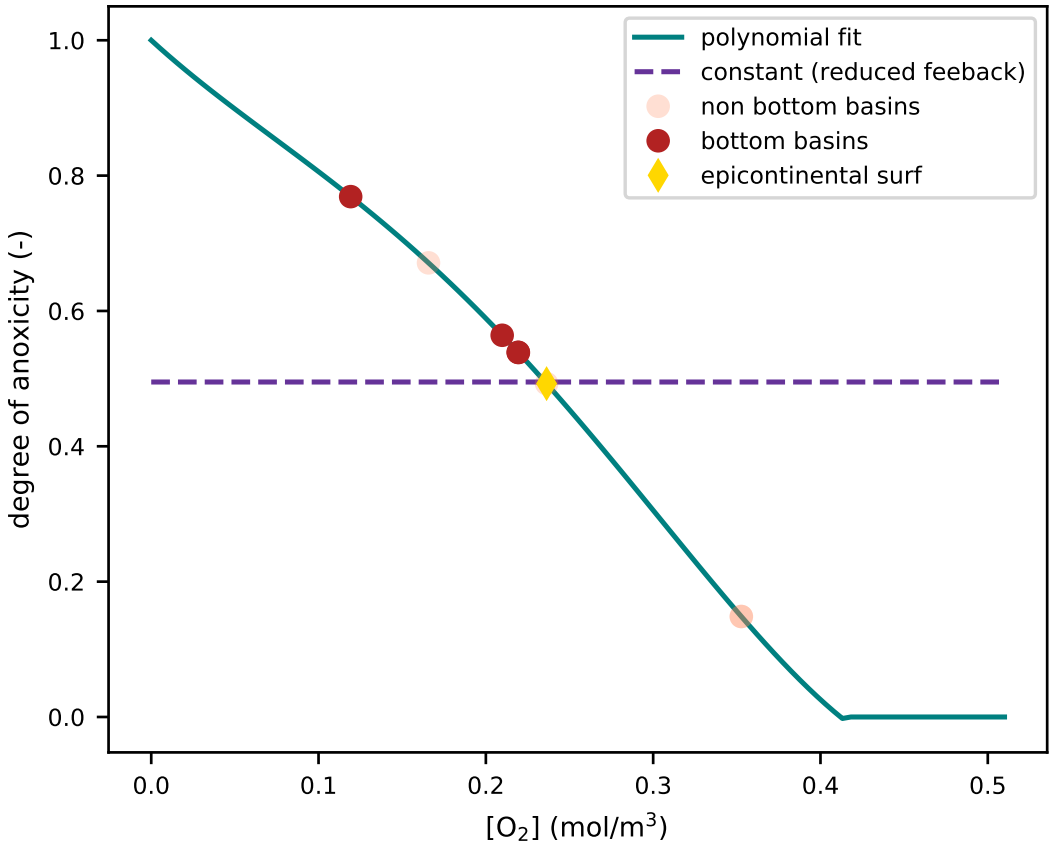

Figure S1. Degree of Anoxicity (DOA) as a function of oceanic O_2 concentration (polynomial fit of (Van Cappellen & Ingall, 1994)). The dashed line represent the value of constant DOA cases ("feedback-1", "feedback-2" and "no-feedback"). Symbols represent the values of COMBINE basins in ERA5-calibration control run.

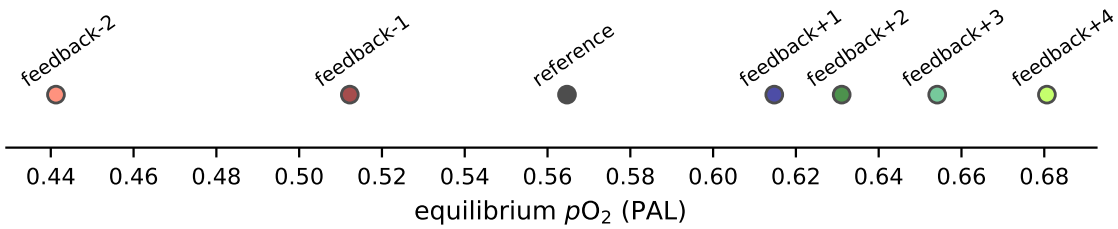

Figure S2. Equilibrium pO_2 after a 50% increase in kerogen weathering (with different feedback strengths), everything else unchanged (including phosphorus and sulfide weathering).

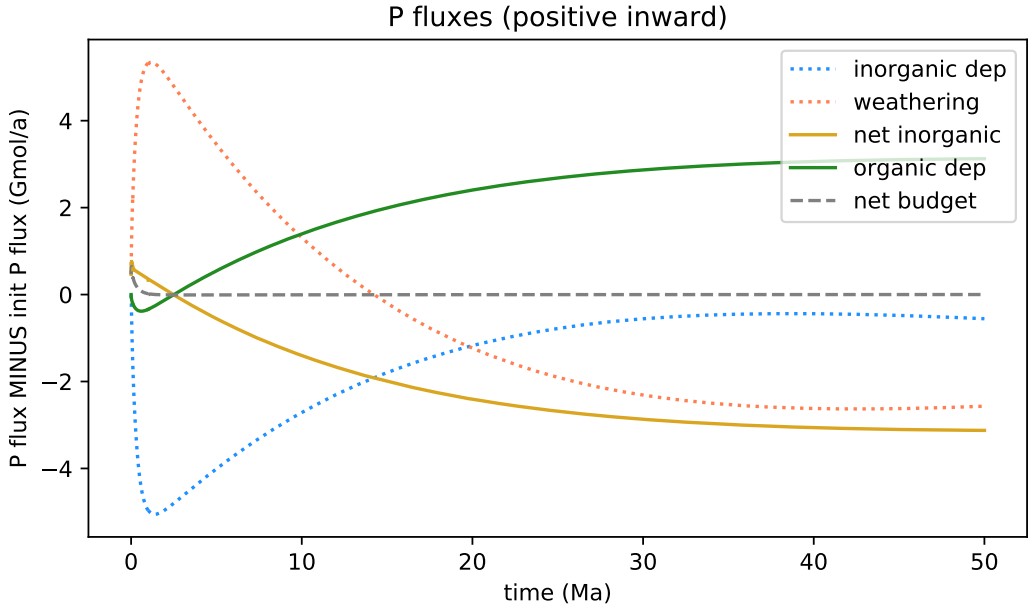

Figure S3. Oceanic phosphorus budget following the perturbation "abrupt carbonate sulfuric weathering" (same as presented in main text) applied at $t = 0$.

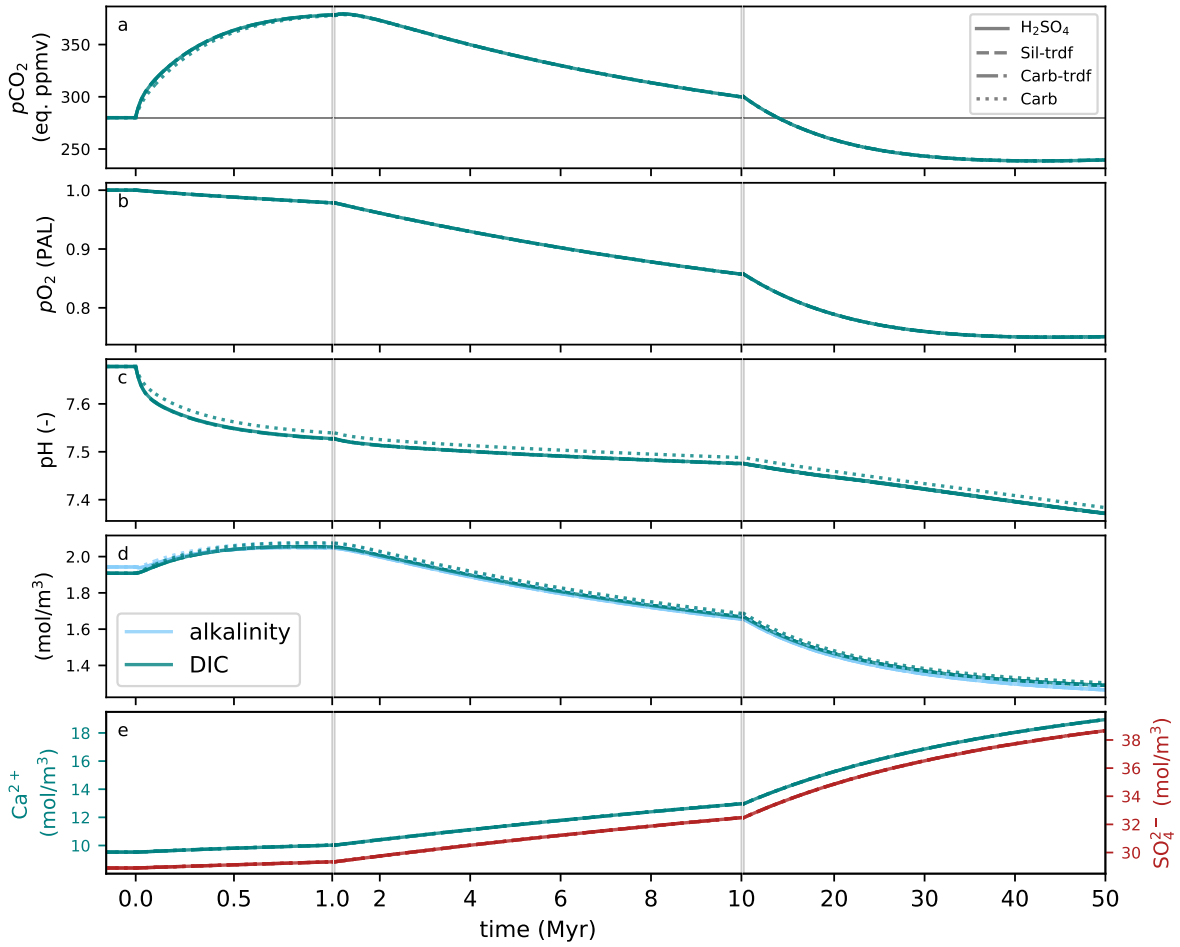

Figure S4. Time evolution of main ocean-atmosphere chemical species following an abrupt perturbation: "H_2SO_4 release", "Silicate trade-off", "Carbonate trade-off" and "Carbonate" (see text S4). The "Carbonate" perturbation is the same as in the main text. The perturbation applied at $t = 0$ and sustained. a. atmospheric CO_2, b. atmospheric O_2, c. mean ocean pH, d. mean ocean Dissolved Inorganic Carbon and alkalinity, e. mean ocean calcium (left) and sulfate (right). The partial pressure of CO_2 in panel a. is expressed in equivalent ppmv, which is its theoretical mixing ratio if all other gases were kept at pre-industrial level. The partial pressure of O_2 is expressed relatively to present atmospheric level (PAL).

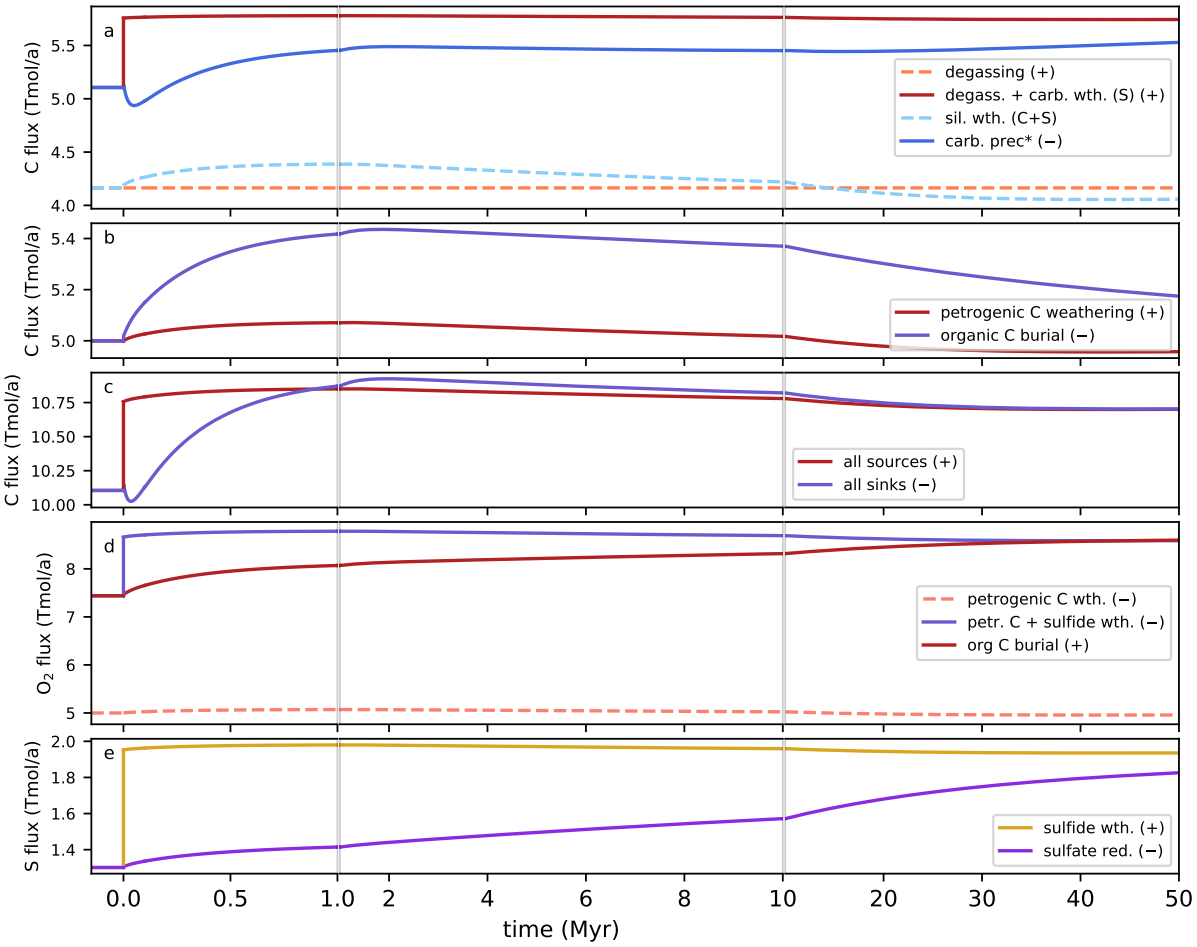

Figure S5. Time evolution of geochemical fluxes following an "abrupt carbonate sulfuric weathering" perturbation applied at $t = 0$. a. inorganic C fluxes, b. organic C fluxes, c. sum of organic and inorganic C fluxes, d. O_2 fluxes, e. sulfate fluxes. When ambiguous, weathering by carbonic or sulfuric acid is specified by C or S (respectively). "carb prec*" in panel a means "carbonate precipitation minus carbonate weathering by carbonic acid". The same subtraction is applied in the sum of fluxes (panel c).

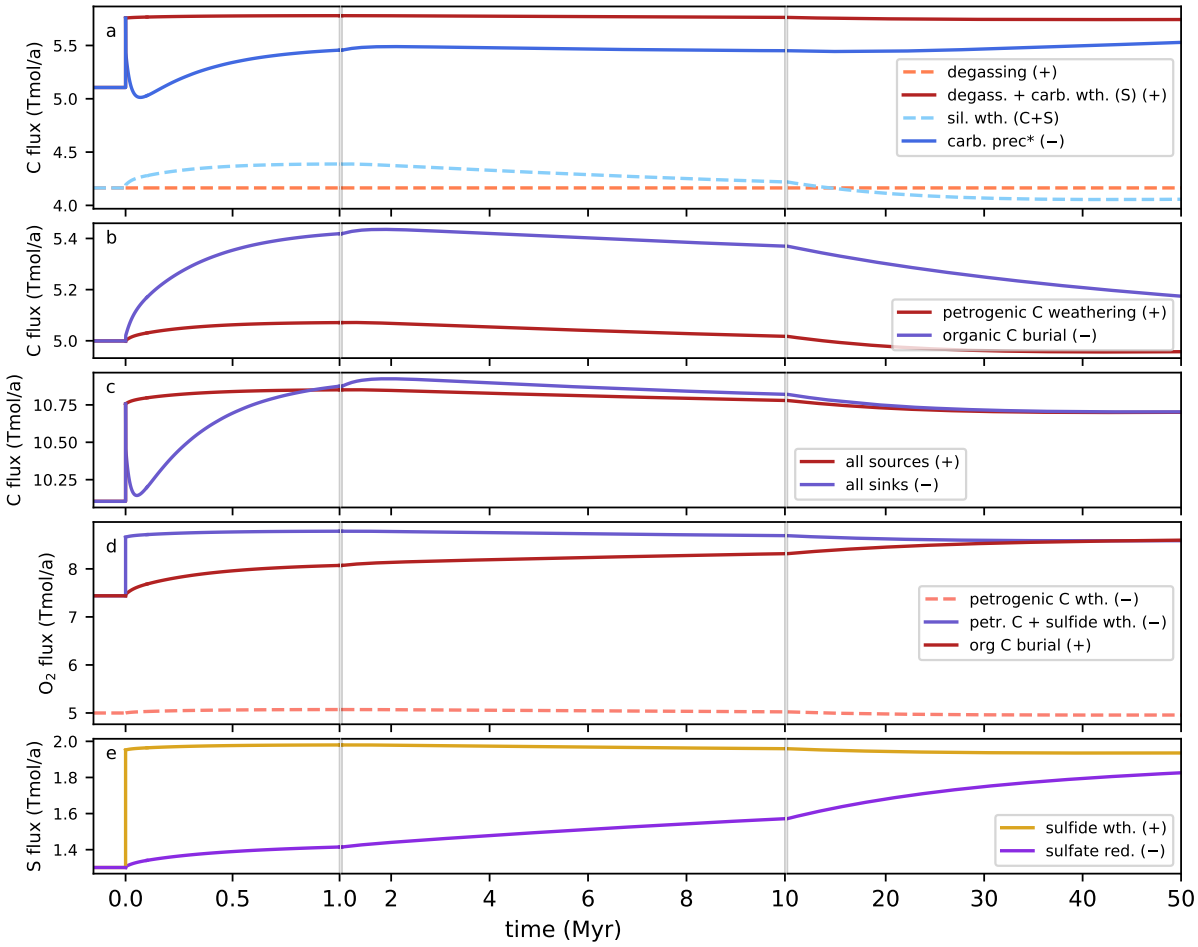

Figure S6. Same as Figure S5 for the abrupt perturbation "Carbonate trade-off"

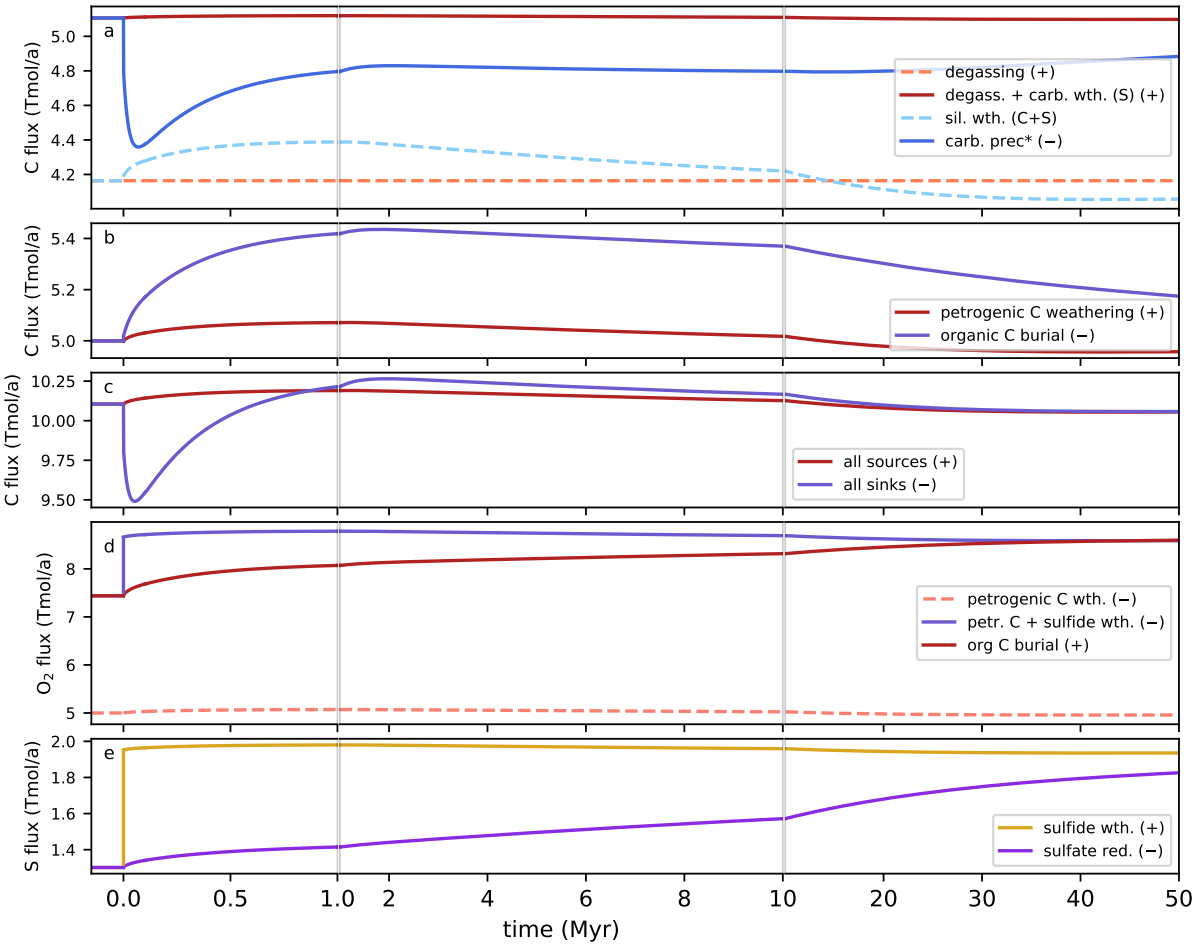

Figure S7. Same as Figure S5 for the abrupt perturbation "Silicate trade-off"

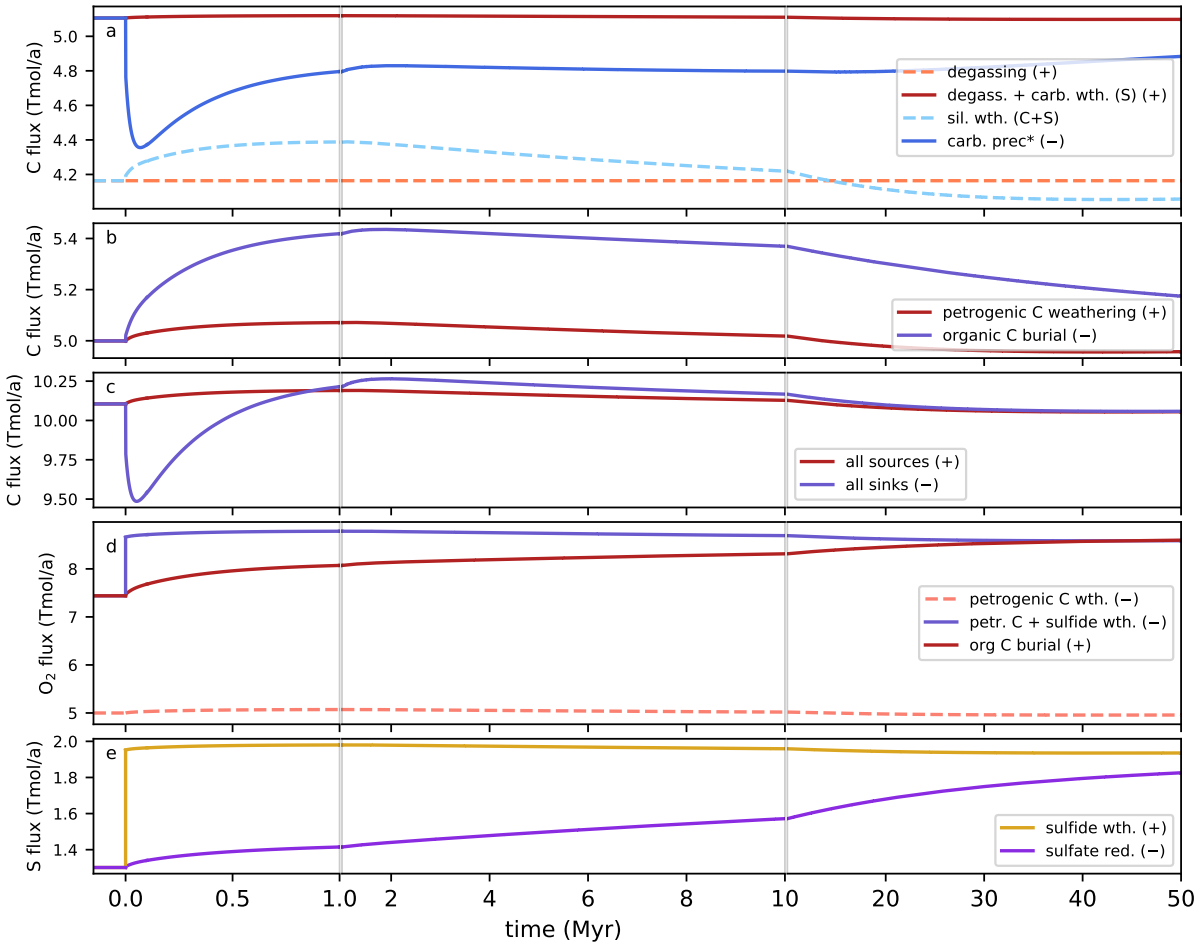

Figure S8. Same as Figure S5 for the abrupt perturbation "H_2SO_4 release"

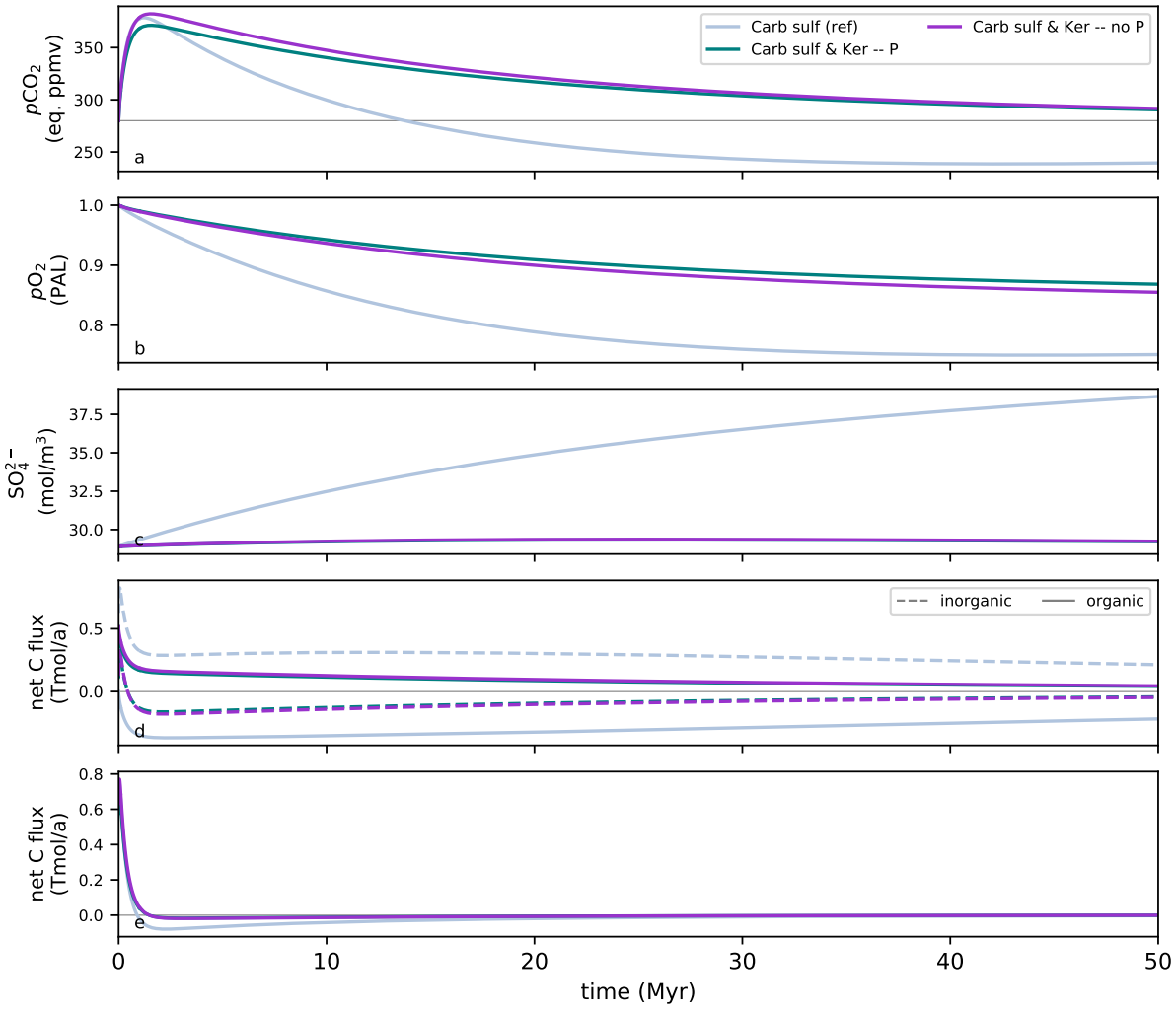

Figure S9. Time evolution of atmospheric CO_2 (a.) and O_2 (b.), oceanic sulfate (c.), net inorganic and organic carbon fluxes (d.) and net carbon flux (e.). 3 simulation setups are presented: 50% increase of sulfide weathering (ref), 10.32% increase of sulfide weathering and kerogen weathering (Carb sulf & ker – P), and same without additional P from kerogen weathering (Carb sulf & ker – P). In each case, the perturbation is applied at $t = 0$, and the additional sulfuric acid dissolves new carbonate minerals. The units of pCO_2 and pO_2 are the same than in Figure S4.

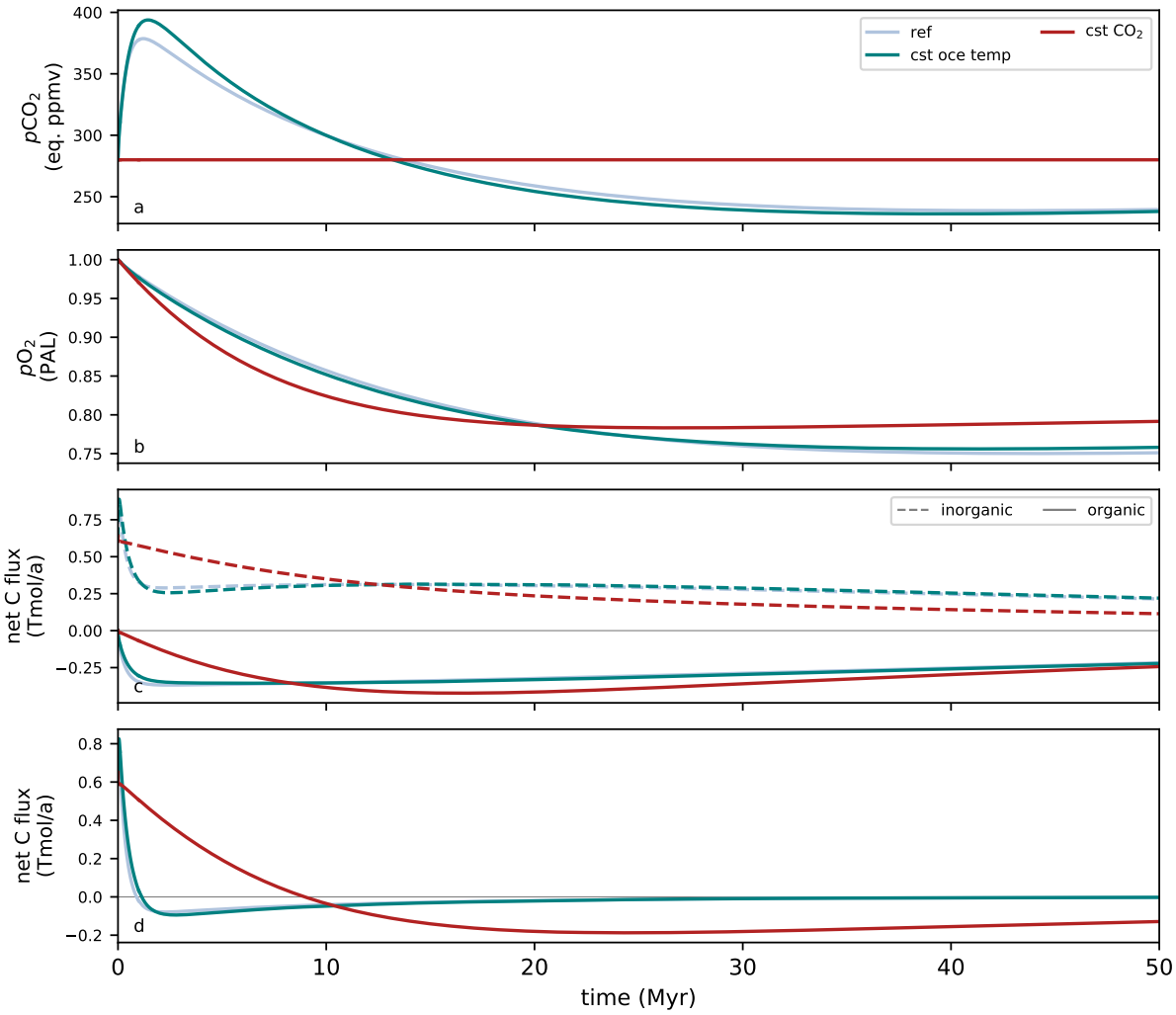

Figure S10. Time evolution of atmospheric CO_2 (a.) and O_2 (b.), net inorganic and organic carbon fluxes (c.) and net carbon flux (d.). 3 simulation setups are presented: 50% increase of sulfide weathering (ref), same with constant oceanic temperature, and same constant climate (CO_2, temperature and runoff). In each case, the perturbation is applied at $t = 0$, and the additional sulfuric acid dissolves new carbonate minerals. The units of pCO_2 and pO_2 are the same than in Figure S4.